The infarcted myocardium solicits GM-CSF for the detrimental oversupply of inflammatory leukocytes

Atsushi Anzai,[1,2] Jennifer L. Choi,[1,2] Shun He,[1,2] Ashley M. Fenn,[1,2] Manfred Nairz,[1,2] Sara Rattik,[1,2] Cameron S. McAlpine,[1,2] John E. Mindur,[1,2] Christopher T. Chan,[1,2] Yoshiko Iwamoto,[1,2] Benoit Tricot,[1,2] Gregory R. Wojtkiewicz,[1,2] Ralph Weissleder,[1,2,3] Peter Libby,[4] Matthias Nahrendorf,[1,2] James R. Stone,[1] Burkhard Becher,[5] and Filip K. Swirski[1,2]

[1]Center for Systems Biology and [2]Department of Radiology, Massachusetts General Hospital and Harvard Medical School, Boston, MA
[3]Department of Systems Biology, Harvard Medical School, Boston, MA
[4]Cardiovascular Division, Department of Medicine, Brigham and Women's Hospital, Boston, MA
[5]Institute of Experimental Immunology, University of Zurich, Zurich, Switzerland

Myocardial infarction (MI) elicits massive inflammatory leukocyte recruitment to the heart. Here, we hypothesized that excessive leukocyte invasion leads to heart failure and death during acute myocardial ischemia. We found that shortly and transiently after onset of ischemia, human and mouse cardiac fibroblasts produce granulocyte/macrophage colony-stimulating factor (GM-CSF) that acts locally and distally to generate and recruit inflammatory and proteolytic cells. In the heart, fibroblast-derived GM-CSF alerts its neighboring myeloid cells to attract neutrophils and monocytes. The growth factor also reaches the bone marrow, where it stimulates a distinct myeloid-biased progenitor subset. Consequently, hearts of mice deficient in either GM-CSF or its receptor recruit fewer leukocytes and function relatively well, whereas mice producing GM-CSF can succumb from left ventricular rupture, a complication mitigated by anti–GM-CSF therapy. These results identify GM-CSF as both a key contributor to the pathogenesis of MI and a potential therapeutic target, bolstering the idea that GM-CSF is a major orchestrator of the leukocyte supply chain during inflammation.

INTRODUCTION

During myocardial infarction (MI), interruption of coronary artery blood flow causes sterile cardiac injury. Although advances in medical and interventional management have improved outcomes after MI, many patients still develop progressive left ventricular dysfunction as a result of myocyte loss, suboptimal healing, and adverse left ventricular remodeling. Thus, beyond current standard revascularization and neurohumoral blockade measures, we urgently need new approaches to minimize acute cardiac ischemic damage and optimize the healing response to maximize the avoidance of chronic ischemic cardiomyopathy.

Wound healing after MI involves a variety of molecular and cellular events that replace necrotic myocardial debris with granulation tissue and a collagen-rich scar (Prabhu and Frangogiannis, 2016). Ischemic injury triggers massive recruitment of BM and spleen-derived neutrophils and monocytes (Nahrendorf et al., 2007; Swirski et al., 2009; Dutta et al., 2012; Leuschner et al., 2012; Swirski and Nahrendorf, 2013; Heidt et al., 2014; Hilgendorf et al., 2014a), which, upon accumulation, contribute to inflammation and repair by producing cytokines, proteases, reactive oxygen species, angiogenic substances, and growth factors. An optimal response should remove the irreversibly damaged myocytes while limiting further ischemic damage and avoiding complications such as heart failure or left ventricular rupture. Understanding the endogenous immune inflammatory mechanisms that operate during MI may identify strategies for avoiding ischemic cardiomyopathy, thus complementing current interventional and neurohumoral blockade approaches.

The multifunctional growth factor GM-CSF controls leukocyte production, proliferation, differentiation, and survival (Bradley and Metcalf, 1966; Hamilton, 2008; Becher et al., 2016). Although hematopoiesis under normal physiological conditions does not require GM-CSF, its production rises substantially after injury, which is one reason that current clinical trials target GM-CSF for diverse inflammatory conditions such as rheumatoid arthritis and multiple sclerosis (Hamilton et al., 2016; Wicks and Roberts, 2016). With the exception of a few inconclusive and contradictory findings, the role of GM-CSF in MI remains largely unresolved. For example, serum GM-CSF levels rise in patients with MI, correlating with severity of acute decompensated heart failure and subsequent cardiac remodeling (Parissis et al., 2000, 2004), whereas exogenous GM-CSF administration exacerbates heart failure (Maekawa et al., 2004). In some patients, however, GM-CSF may be beneficial after MI by improving

Correspondence to Filip K. Swirski: fswirski@mgh.harvard.edu

Abbreviations used: MI, myocardial infarction; MMP, matrix metalloproteinase; MRI, magnetic resonance imaging.

The Rockefeller University Press
J. Exp. Med. 2017 Vol. 214 No. 11 3293–3310
https://doi.org/10.1084/jem.20170689

neoangiogenesis (Seiler et al., 2001; Bruno et al., 2006). Here, we explored GM-CSF's function in MI using human tissue and mice deficient in GM-CSF or its receptor (GM-CSFR). We demonstrate that GM-CSF impairs healing after MI by acting locally in the heart and at a distance in the BM to produce and recruit inflammatory leukocytes.

RESULTS

GM-CSF is detrimental in MI

To explore GM-CSF's function after MI, we first evaluated postinfarction survival. We found that WT mice died of cardiac rupture in considerably higher numbers than *Csf2*$^{-/-}$ mice (Fig. 1 A). Among survivors, *Csf2*$^{-/-}$ mice had improved left ventricular systolic function 21 d after MI, as assessed by cardiac magnetic resonance imaging (MRI), despite similar initial (1 d post-MI) infarct size or left ventricular volume in the groups (Fig. 1, B and C; and Fig. S1 A). On histological examination, 7-d-old infarcts of *Csf2*$^{-/-}$ mice had reduced CD11b^{+} myeloid cell numbers, reduced collagen accumulation, and smaller α smooth muscle actin areas, with no differences in CD31^{+} endothelial cell number (Fig. 1 D), whereas flow cytometry revealed attenuated neutrophil, Ly-6C^{high} monocyte, and macrophage accumulation in *Csf2*$^{-/-}$ hearts 3 and 7 d after MI (Fig. 1, E and F). At day 3, compared with WT, infarcts in *Csf2*$^{-/-}$ mice had much lower levels of mRNAs that encode inflammatory cytokines such as IL-1β, IL-6, and matrix metalloproteinase (MMP)-9 (Fig. 1 G). Though GM-CSF may promote macrophage apoptosis through IL-23 (Subramanian et al., 2015), we found no differences in IL-23 mRNA levels in the infarct (Fig. 1 G). Mice lacking the common β subunit of the GM-CSF receptor (CD131; Csf2rb) yielded similar results (Fig. S1 B). Administration of recombinant mouse GM-CSF to WT mice decreased survival while increasing leukocyte accumulation (Fig. 1, H and I), whereas administration of anti-GM-CSF neutralizing antibody protected WT mice from cardiac rupture and improved survival during the first 4 wk after permanent coronary ligation (Fig. 1 J). These data suggest that endogenous GM-CSF causes impaired wound healing resulting from aggravated inflammation and enhanced leukocyte accumulation after MI.

Cardiac fibroblasts produce GM-CSF in response to acute ischemic injury in both mice and humans

The striking improvements in survival and cardiac function, along with the attenuated inflammation, in mice lacking GM-CSF, prompted us to delve deeper into the orchestrating mechanisms. The infarct, and not the uninfarcted myocardium, spleen, BM, and lymph nodes, augmented *Csf2* mRNA, which peaked on day 1 and subsided thereafter (Fig. 2 A), suggesting a direct link between point of injury and GM-CSF induction. Expression of *Il3* and *Il5*, the growth factors that also signal to Csf2rb, were undetectable and unchanged, respectively, indicating an exclusive and dynamic GM-CSF/GM-CSFR signaling dyad after MI (Fig. 2 B). Infarcted tissue also produced abundant Csf2 protein in both WT and *Csf2rb*$^{-/-}$ mice (Fig. 2 C), reflecting robust local translation independent of GM-CSF signaling. That *Csf2*$^{-/-}$ mice did not produce any GM-CSF confirmed the integrity of the mouse strain and the assays used (Fig. 2 C).

The presence of the GM-CSF transcript in the heart argued in favor of the idea of a cardiac-resident cell population as the growth factor's source. Using FACS, we identified four cell types in the heart (Fig. 2 D): leukocytes, which express CD45; endothelial cells, which do not express CD45 but are abundant for CD31; fibroblasts, which express the fibroblast-specific marker MEFSK4 (Pinto et al., 2016), along with other classic fibroblast-associated markers (Fig. 2, D and E); and so-called other stromal cells, which lack the aforementioned markers and thus comprise a mixture of cells, some of which are cardiomyocytes (Fig. 2, D and F). Strikingly, fibroblasts were the most abundant, and nearly exclusive, Csf2 producers 1 d after coronary artery ligation (Fig. 2 G), with minor production by other cells and no production otherwise. The increase depended on a mixture of danger-associated molecular patterns given reduced GM-CSF production in *Myd88*$^{-/-}$, *Tlr9*$^{-/-}$, and *Ticam1*$^{-/-}$ mice (Fig. 2 H). To test whether cardiac fibroblasts can directly sense danger signals via TLR3 and TLR9, we sorted fibroblasts, placed them in culture, stimulated with the two TLR ligands alone or in combination, and measured GM-CSF in supernatants. Our in vitro data confirm that fibroblasts can produce GM-CSF through Ticam1-dependent (Tlr3) and Myd88-dependent (Tlr9) mechanisms, suggesting the importance of multiple signals for GM-CSF production (Fig. 2 I).

The data obtained in the mouse led us to consider whether infarcted human hearts likewise produce GM-CSF after MI. We obtained heart tissue specimens from deceased patients with infarcts that, upon pathological examination, were classified as acute (1–2 d because of C4d staining) or late (5–7 d, given signs of leukocyte accumulation and granulation tissue formation). We also examined hearts from patients who died from causes unrelated to MI. Consistent with data obtained in the mouse, we found that the acutely infarcted myocardium, and not the late infarct or the uninfarcted myocardium, contained GM-CSF^{+} cells. Of these, the majority were spindle-shaped cells that expressed vimentin, a morphology and phenotype consistent with cardiac fibroblasts (Fig. 2, J–L). These data indicate that cardiac fibroblasts predominate as the source of GM-CSF in the acutely infarcted myocardium in both mice and humans.

GM-CSF recruits leukocytes after MI by stimulating chemokine production

Having established GM-CSF's source, we next sought to determine whether GM-CSF influences the response to ischemic injury via local effects in the heart. Because of the correlation between GM-CSF expression and leukocyte accumulation, we reasoned that the growth factor may contribute to leukocyte accrual, which depends on influx, survival,

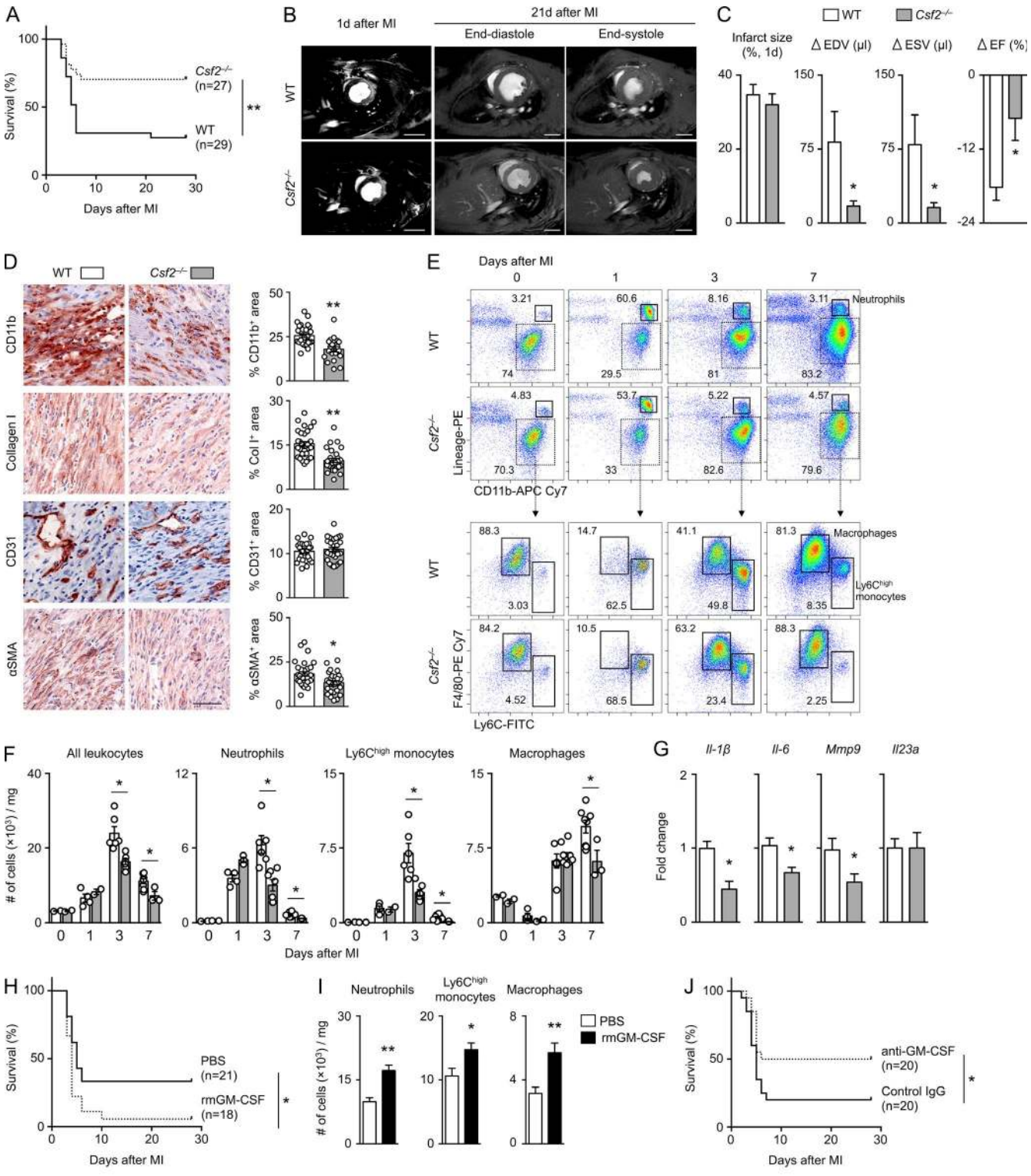

Figure 1. **GM-CSF is detrimental in MI.** (A) Post-MI survival rate in WT and *Csf2*$^{-/-}$ mice. Data are from three independent experiments. **, P < 0.01. (B) Representative MRI images showing infarct size with late gadolinium enhancement on 1 d and heart morphology at end-diastolic and end-systolic phases 21 d after MI in WT and *Csf2*$^{-/-}$ mice. Bars, 4 mm. (C) Quantification of infarct size at 1 d as well as individual changes in indicated parameters from 1 to 21 d post-MI (n = 6–7 per group from two independent experiments). *, P < 0.05. (D) Immunohistochemical study of infarcted tissue for CD11b, collagen I, CD31, and α-smooth muscle actin (αSMA) in WT and *Csf2*$^{-/-}$ mice 7 d after MI. Quantification of 10 randomly assigned fields of view per sample (n = 5 per group). Bar, 30 µm. *, P < 0.05; **, P < 0.01. (E) Representative flow dot plots of MI tissue cell suspensions before and 1, 3, and 7 d after MI in WT and

and proliferation. We eliminated the likelihood that GM-CSF promotes leukocyte survival (Fig. 3, A and B) and proliferation (Fig. 3 C), and thus focused on influx. We found that 3-d-old infarcts in *Csf2*$^{-/-}$ mice expressed lower levels of *Cxcl2*, *Ccl2*, *Ccl3*, *Ccl5*, and *Ccl7* compared with WT mice (Fig. 3 D). Among those chemokines that are GM-CSF dependent, Cxcl2 attracts neutrophils whereas Ccl2, Ccl3, Ccl5, and Ccl7 attract Ly-6C^{high} monocytes. Because we found no differences in expression of either neutrophil Cxcr2 (ligand for Cxcl2) or monocyte Ccr2 (ligand for Ccl2) between WT and *Csf2rb*$^{-/-}$ mice (Fig. 3 E), we concluded that GM-CSF–dependent effects on recruitment, if any, likely rely on the attracting chemokines produced in the heart.

To explore neutrophil recruitment, we profiled Cxcl1 and Cxcl2. We found that cardiac fibroblasts produced abundant levels of GM-CSF–independent Cxcl1, whereas leukocytes were the largest source of GM-CSF–dependent Cxcl2 (Fig. 4 A). Among the leukocytes, neutrophils generated considerable Cxcl2, and *Csf2rb*$^{-/-}$ neutrophils expressed significantly less Cxcl2 compared with WT cells (Fig. 4 B). These data collectively indicate that enhanced neutrophil accumulation is a function of increased recruitment rather than survival. This recruitment is driven by GM-CSF, which stimulates neutrophil-attracting Cxcl2 production.

To explore monocyte recruitment, we profiled Ccl2. To determine Ccl2's cellular source after MI, we took advantage of Ccl2 reporter mice, in which all Ccl2^{+} cells express the fluorescent protein mCherry. mCherry^{+} cells appeared in 2-d-old infarcts, with minimal to no expression in naive hearts, blood cells, or cells in the BM (Fig. 4 C). Among the cardiac Ccl2 producers, myeloid cells, such as Ly-6C^{high} monocytes and macrophages, predominated, with additional contribution from neutrophils and cardiac fibroblasts (Fig. 4, C and D). In *Ccr2*$^{-/-}$ mice, which have profoundly reduced numbers of circulating monocytes, Ccl2 production in the heart was diminished, along with diminished monocyte and macrophage accumulation, further substantiating the idea that monocytes are Ccl2 sources (Fig. 4 E). Ccl2 production depended on signaling via GM-CSFR (Fig. 4 F), thus recapitulating observations made in *Csf2*$^{-/-}$ mice (Fig. 3 D). In vitro, GM-CSF strongly stimulated Ccl2 production from sorted Ly-6C^{high} monocytes and macrophages. We also profiled cells from *Csf2rb*$^{-/-}$ mice as controls and found no Ccl2 production in response to GM-CSF, indicating a direct, specific stimulation (Fig. 4 G). However, neither neutrophils nor fibroblasts produced additional Ccl2 upon GM-CSF stimulation, indicating that Ccl2 production in these cells involves GM-CSF–independent pathways. To dig deeper, we found phosphorylated STAT5 in Ly-6C^{high} monocytes and macrophages, indicating GM-CSF signaling (Fig. 4 H). Finally, we adoptively transferred Ly-6C^{high} monocytes from GFP^{+} mice into WT and *Csf2*$^{-/-}$ animals subjected to coronary ligation 3 d earlier. Even though the same number of GFP^{+} cells were injected, we retrieved far fewer GFP^{+} cells from *Csf2*$^{-/-}$ infarcts (Fig. 4, I and J). Our data show that cardiac GM-CSF attracts monocytes to the heart by stimulating Ccl2 production.

GM-CSF promotes accumulation of proteolytic and inflammatory neutrophils and monocytes after MI

Our data thus far indicate that GM-CSF promotes leukocyte influx to the infarcted myocardium via neutrophil- and monocyte-attracting chemokine production. We next tested whether GM-CSF influences leukocyte function. We elected to profile inflammatory and proteolytic activity, as these can disrupt wound repair (Nahrendorf et al., 2007; Hilgendorf et al., 2014a) and contribute to left ventricular heart rupture (Heymans et al., 1999; Matsumura et al., 2005), respectively. Using a probe that reports on proteolytic activity (Nahrendorf et al., 2007), we found considerably reduced proteolysis in *Csf2*$^{-/-}$ mice (Fig. 5, A and B). Among the cells, Ly6C^{high} monocytes and neutrophils contributed comparably to proteolysis, but the highest proteolytic activity tracked with macrophages (Fig. 5, C and D). Importantly, all three cell types had reduced proteolytic activity in *Csf2*$^{-/-}$ mice. In keeping with these observations, we likewise detected reduced expression of *Il1β*, *Il6*, and *Mmp9* in sorted neutrophils, Ly-6C^{high} monocytes, and macrophages of *Csf2rb*$^{-/-}$ mice, compared with WT mice (Fig. 5 E). Together, these data indicate that GM-CSF not only induces monocyte and neutrophil influx but is also important to leukocyte function, including proteolysis and inflammation.

GM-CSF stimulates BM hematopoiesis by acting on CD131^{+} multipotent progenitors after MI

Having shown the local action of GM-CSF, we next considered whether the growth factor also acts systemically. In support of this idea, GM-CSF protein levels increased in serum and BM 1 and 2 d after coronary artery ligation (Fig. 6, A and B). To determine whether heart-derived GM-CSF can influence the BM via the circulation, we joined WT mice

Csf2$^{-/-}$ mice. (F) Flow cytometry–based quantification of indicated cells in the hearts of WT and *Csf2*$^{-/-}$ mice before and 1, 3, and 7 d after MI (n = 3–7 per group from at least two independent experiments). *, $P < 0.05$. (G) mRNA levels of indicated cytokines in the infarcted tissue of WT and *Csf2*$^{-/-}$ mice 3 d after MI (n = 5–8 per group from three independent experiments). *, $P < 0.05$. (H) Post-MI survival rate in recombinant mouse GM-CSF (rmGM-CSF)-injected and PBS-injected WT mice. Data are from three independent experiments. *, $P < 0.05$. (I) Flow cytometry–based quantification of indicated cells in the hearts of rmGM-CSF–injected and PBS-injected WT mice 3 d after MI (n = 7 per group from three independent experiments). *, $P < 0.05$; **, $P < 0.01$. (J) Post-MI survival rate in mice treated with anti–GM-CSF neutralization antibody and control IgG. Data are from three independent experiments. *, $P < 0.05$. For statistical analysis, log-rank test was applied to compare survival curves, and two-tailed unpaired t test was performed to compare two groups. Results are shown as mean ± SEM.

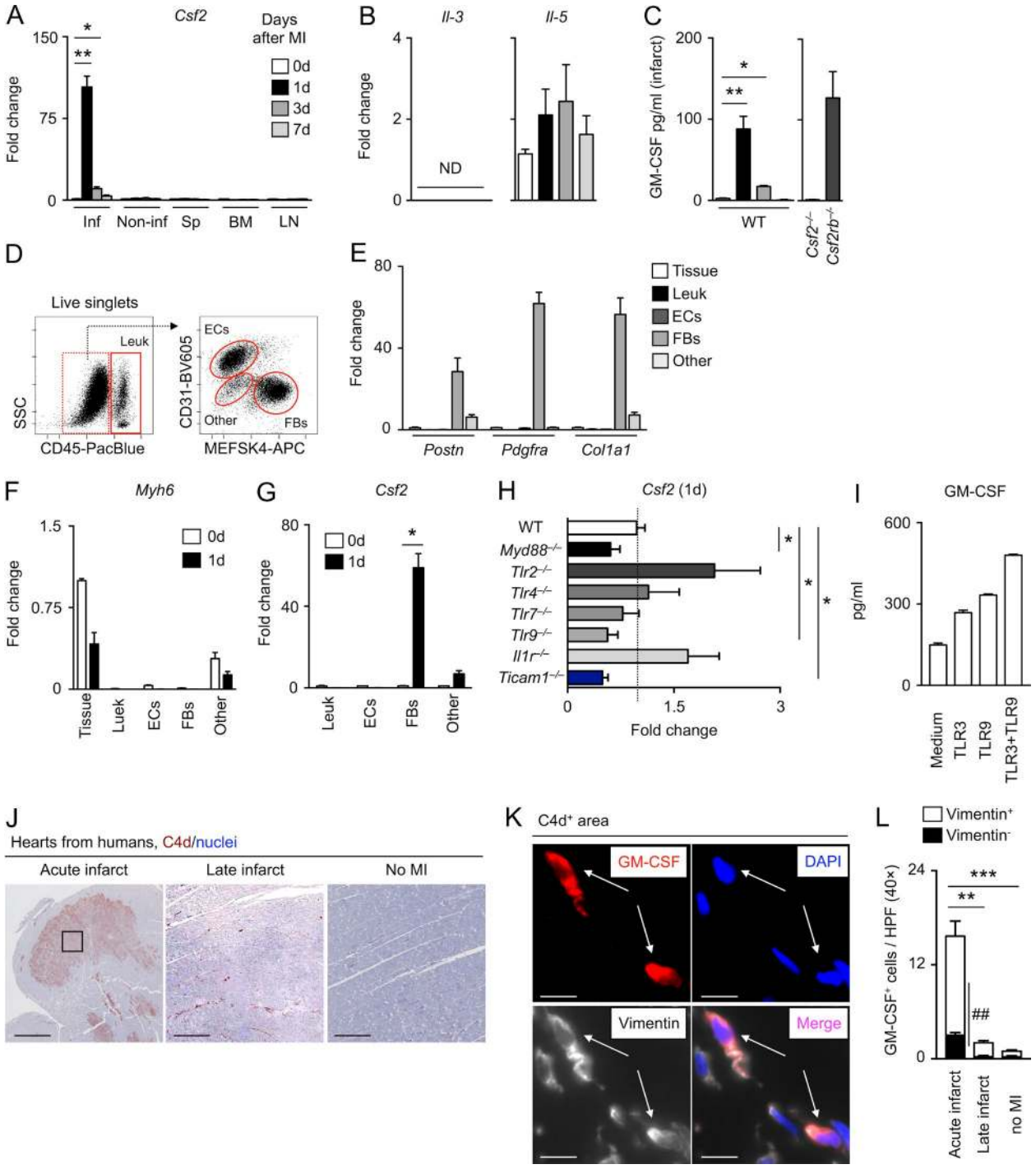

Figure 2. **GM-CSF is produced by cardiac fibroblasts after MI in mice and humans.** (A) *Csf2* mRNA levels in the infarcted tissue, uninfarcted tissue, spleen, BM, and mediastinal lymph node 1, 3, and 7 d after MI. Control mice were analyzed before MI (day 0; n = 3–5 per group from at least two independent experiments). *, $P < 0.05$, **, $P < 0.01$ vs. control. (B) *Il-3* and *Il-5* mRNA expression levels in infarcted tissue 1, 3, and 7 d after MI. Control mice were analyzed before MI (day 0; n = 5–6 per group from two independent experiments). (C) GM-CSF protein concentration in the heart homogenate of WT, *Csf2*$^{-/-}$, and *Csf2rb*$^{-/-}$ mice 1, 3, and 7 d after MI. Control mice were analyzed before MI (day 0; n = 3–5 per group from two independent experiments) *, $P < 0.05$, **, $P < 0.01$ vs. control. (D) Flow cytometric gating strategy to determine total leukocytes (Leuk), endothelial cells (ECs), fibroblasts (FBs), and other stromal cells (Other) in the heart. (E) Expression levels of genes encoding periostin (*Postn*), platelet-derived growth factor receptor-α (*Pdgfra*), and collagen 1a1 (*Col1a1*) in infarcted tissue and indicated cells sorted from infarcted myocardium 1 d after MI. Values are normalized by gene levels in tissue (n = 5–6 per group from two independent experiments). (F) Gene levels of *Myh6*, which is specific for cardiomyocytes, in the heart tissue and the sorted heart subpopulations defined in D before and 1 d after MI. Data were normalized to 0 d tissue (n = 5–6 per group from two independent experiments).

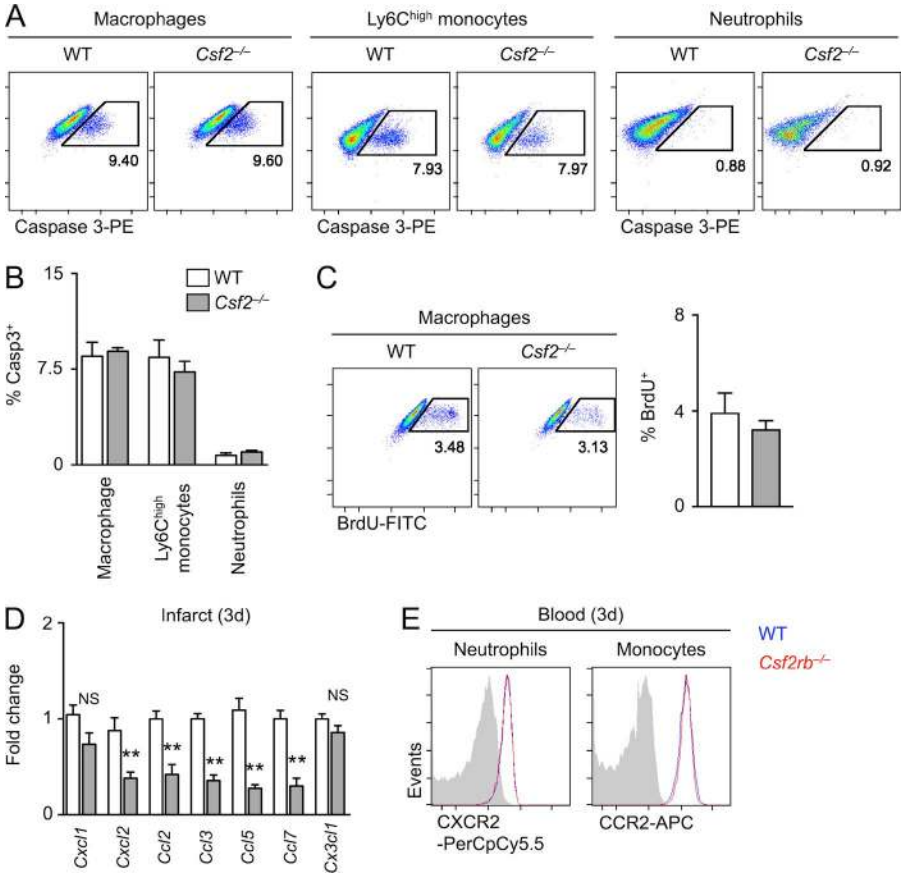

Figure 3. **GM-CSF promotes chemokine expression, but does not affect cell survival and proliferation in infarcted myocardium.** (A) Representative flow cytometric dot plots of activated caspase 3 expression in WT and *Csf2*$^{-/-}$ macrophages, Ly-6C^{high} monocytes, and neutrophils in infarcted tissue 3 d after MI. (B) Flow cytometry–based quantification of activated caspase 3^{+} cells shown in A (n = 4 per group from two independent experiments). (C) Flow cytometric analysis of BrdU incorporation into WT and *Csf2*$^{-/-}$ macrophages in the infarcted tissue 3 d after MI. BrdU was injected 2 h before death (n = 5 per group from two independent experiments). (D) Gene expression levels of *Cxcl1*, *Cxcl2*, *Ccl2*, *Ccl3*, *Ccl5*, *Ccl7*, and *Cx3cl1* in 3-d-old infarcts of WT and *Csf2*$^{-/-}$ mice (n = 7–8 per group from three independent experiments). **, P < 0.01; NS, not significant. (E) Representative flow cytometric histograms for CXCR2 expression on blood neutrophils and CCR2 expression on blood Ly-6C^{high} monocytes of WT and *Csf2rb*$^{-/-}$ mice 3 d after MI. For statistical analysis, two-tailed unpaired t test was performed to compare two groups. Results are shown as mean ± SEM.

with either WT or *Csf2rb*$^{-/-}$ partners by parabiosis, waited 14 d to establish equilibrium (Theurl et al., 2016), subjected the WT mouse to coronary ligation, and performed a 2-h BrdU pulse-chase experiment 2 d later (Fig. 6 C). Compared with non-MI controls, we found higher Ly-6C^{high} monocyte production rates in WT partner BM (i.e., WT partner of a WT mouse that underwent coronary ligation), indicating that MI can stimulate hematopoiesis via the blood. *Csf2rb*$^{-/-}$ partners, in contrast, showed blunted production (Fig. 6 C), indicating that infarct-derived GM-CSF travels through the circulation to stimulate BM hematopoiesis.

To elucidate GM-CSF's specific target, we examined CD131 (i.e., Csf2rb) expression among hematopoietic stem progenitor cells and found a distinct CD131^{+} population within Lin^{-}ckit^{+}Sca1^{+} LSK that was flk2^{-}CD48^{+}CD150^{-}, and thus akin to the recently described myeloid-biased MPP3s (Pietras et al., 2015; Fig. 7 A and Fig. S2). In vitro experiments using different LSK subpopulations stimulated with GM-CSF supported this observation and further revealed that MPP3s responded most to GM-CSF (Fig. 7 B), giving rise to GMP and MDP (Fig. 7 C) before becoming CD11b^{+} mature myeloid cells, comprised of monocytes/macrophages (CD11b^{+} CD115^{+} Ly6G^{-}) and neutrophils (CD11b^{+} CD115^{-}Ly6G^{+}; Fig. 7 D). In vivo, CD131^{+} MPP3s augmented proliferation in WT mice 2 d after MI, whereas CD131^{-} MPP3s and CD131^{+} (and CD131^{-}) MPP3s from *Csf2*$^{-/-}$ mice proliferated at baseline rates (Fig. 7 E). In agreement with these data, *Csf2rb*$^{-/-}$ mice had a lower

(G) *Csf2* mRNA expression levels in the sorted heart subpopulations defined in D before and 1 d after MI (n = 4–5 mice from at least two independent experiments). *, P < 0.05 vs. 0 d. (H) *Csf2* mRNA expression levels in infarcted tissue of WT, *Myd88*$^{-/-}$, *Tlr2*$^{-/-}$, *Tlr4*$^{-/-}$, *Tlr7*$^{-/-}$, *Tlr9*$^{-/-}$, *Il1r*$^{-/-}$, and *Ticam1*$^{-/-}$ (the gene that encodes TRIF) mice 1 d after MI (n = 4–8 mice from two to three independent experiments). *, P < 0.05 vs. WT heart. (I) GM-CSF protein concentration in supernatants of cardiac fibroblasts cultured in the presence or absence of TLR3 or TLR9 agonists (n = 4–6 per group from at least two independent experiments). (J) Representative immunohistochemical images of C4d staining in heart sections of patients with or without MI. Acute and late infarcts indicate the heart sections from patients who died within 2 d (acute) or 7 d (late) after MI onset. Bars, 1 mm. (K) Identification of GM-CSF^{+} vimentin^{+} cardiac fibroblasts (white arrows) in C4d^{+} area indicated by the square in J. Bars, 20 µm. (L) Quantification of GM-CSF^{+} cells in heart sections of patients with or without MI. Cells were counted in 25 randomly selected fields of view per sample. **, P < 0.01, ***, P < 0.001 vs. no MI; ##, P < 0.01 vs. vimentin^{-}. For statistical analysis, two-tailed unpaired t test was performed to compare two groups, and one-way ANOVA followed by Tukey's test was performed for multiple comparisons. Results are shown as mean ± SEM.

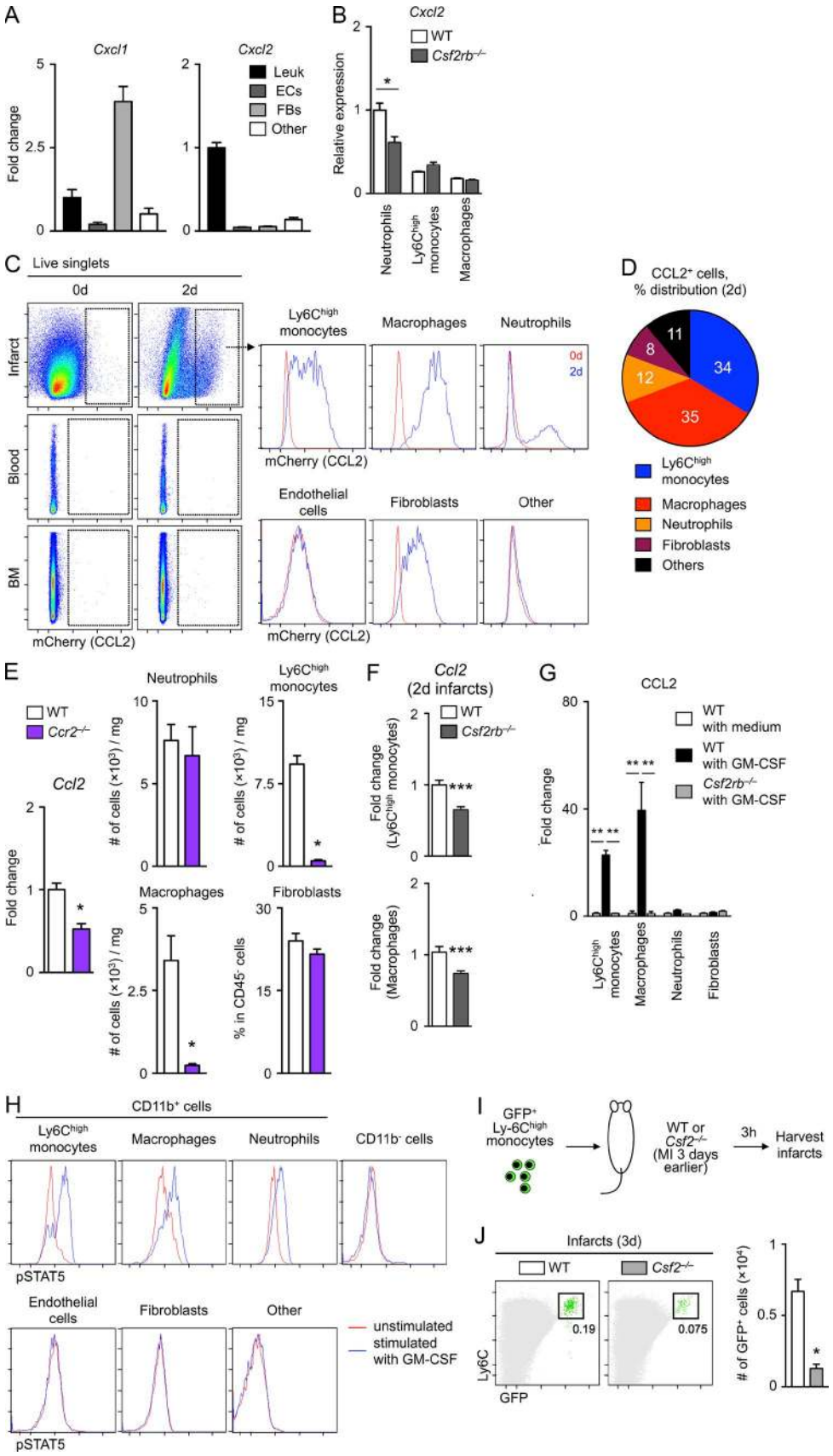

percentage of $BrdU^+$ BM MPP3s than WT mice 2 d after coronary artery ligation (Fig. 7 F). Moreover, experiments involving competitive adoptive transfer of $CD131^+$ and $CD131^-$ MPP3s into WT mice with MI revealed a higher proportion of myeloid cells accumulating in the myocardium that had differentiated from the $CD131^+$ population, suggesting that $CD131^+$ MPP3s have an enhanced capacity for recruitment and differentiation into mature myeloid cells in response to myocardial ischemia (Fig. 7 G). Consequently, the BM of WT mice had more neutrophils and Ly-$6C^{high}$ monocytes during MI than the BM of *Csf2*$^{-/-}$ and *Csf2rb*$^{-/-}$ mice (Fig. 7 H and Fig. S2 B).

We have previously demonstrated that the spleen contributes monocytes to the infarcted myocardium 1 d after MI (Swirski et al., 2009). In this study, we wondered whether the spleen may be contributing to accumulation on day 3, a time point at which we detected GM-CSF–dependent differences. Whereas splenectomy at the time of infarction recapitulated the contribution of the reservoir in the early monocyte response on day 1, splenectomy on day 2 showed no contribution of the spleen to leukocyte accumulation on day 3, indicating that GM-CSF–dependent leukocyte accumulation was spleen independent (Fig. S3, A and B). In agreement with these observations, neutrophils and Ly-$6C^{high}$ monocytes in the spleen were not altered in the absence of GM-CSF signaling 3 d after MI (Fig. S3 C). Together, these data reveal that GM-CSF produced in the heart can promote hematopoiesis in the BM by targeting a specific resident progenitor subset.

GM-CSF licenses BM-derived cells to cause left ventricular rupture and immunopathology after coronary artery ligation

Our data thus far indicate that GM-CSF alerts the hematopoietic compartment for increased inflammatory cell production and recruitment after MI. We next sought to determine whether hematopoietic cells were indeed responsible for the difference in survival between WT and *Csf2*$^{-/-}$ mice, as depicted in Fig. 1. To this end, we generated three types of BM chimeras: lethally irradiated WT mice reconstituted with WT or *Csf2rb*$^{-/-}$ BM cells (hereafter termed WT^{WT} and $WT^{Csf2rb-/-}$, respectively) and lethally irradiated *Csf2rb*$^{-/-}$ mice reconstituted with WT BM cells (*Csf2rb*$^{-/-WT}$). After coronary artery ligation, we observed increased *Csf2* in WT^{WT} mice (Fig. 8 A), along with abundant leukocyte, neutrophil, and Ly-$6C^{high}$ monocyte accumulation in both WT^{WT} and *Csf2rb*$^{-/-WT}$ mice (Fig. 8 B). In contrast, fewer leukocytes accumulated in $WT^{Csf2rb-/-}$ mice, suggesting that GM-CSF–dependent increases in leukocyte numbers were linked directly to hematopoiesis. To test this conjecture, we enumerated cells in the BM, and observed that BM cells lacking the GM-CSF receptor failed to generate progenitors and mature myeloid cells in addition to those generated in the basal state (Fig. 8 C). Moreover, infarcts of $WT^{Csf2rb-/-}$ mice contained lower mRNAs encoding the inflammatory mediators *Il-1β*, *Il-6*, *Mmp9*, and *Ccl2* than those in the other groups (Fig. 8 D). Finally, when followed for 4 wk after coronary ligation, $WT^{Csf2rb-/-}$ mice survived longer compared with the other two groups (Fig. 8 E). Collectively, these data indicate that GM-CSF reduces survival by acting on hematopoietic cells.

DISCUSSION

Many studies have implicated leukocytosis, and specifically the rise of neutrophils and monocytes, as independent risk factors in cardiovascular disease (Kyne et al., 2000; Brown et al., 2001; Hajj-Ali et al., 2001; Maekawa et al., 2002; Madjid et al., 2004; Tsujioka et al., 2009; Nahrendorf et al., 2010). In experimental MI, excessive myeloid cell accumulation likely contributes to adverse cardiac remodeling and death (Panizzi et al., 2010; Kempf et al., 2011; Anzai et al., 2012), whereas hearts with reduced leukocyte infiltration heal and function better than controls (Romson et al., 1983; Kaikita et al., 2004; Leuschner et al., 2010). *Apoe*$^{-/-}$ mice, which develop monocytosis (Swirski et al., 2007) by augmenting responsiveness to GM-CSF (Murphy et al., 2011), have detrimental wound healing and accelerated heart failure after MI (Panizzi et al.,

Figure 4. **GM-CSF recruits neutrophils and monocytes after MI by stimulating Cxcl2 and Ccl2 production.** (A) Gene levels of *Cxcl1* and *Cxcl2* in the sorted heart subpopulations 3 d after MI. Data were normalized to Leuk ($n = 4$ per subpopulation from two independent experiments). (B) *Cxcl2* mRNA expression levels in neutrophils, Ly-$6C^{high}$ monocytes, and macrophages sorted from 3-d-old infarcts of WT and *Csf2rb*$^{-/-}$ mice ($n = 6$ per population from at least two independent experiments). *, $P < 0.05$. (C) Representative flow cytometric images for mCherry expression in B6.Cg-$Ccl2^{tm1.1Pame}$/J mouse heart, blood, and BM before and 2 d after MI. (D) Pie chart showing percentage distribution of $mCherry^+$ cells for the indicated subpopulations in infarcted myocardium 2 d after MI. (E) *Ccl2* mRNA expression in infarct and enumeration of indicated cells in the hearts of WT and *Ccr2*$^{-/-}$ mice 3 d after MI ($n = 4$–6 per group from two independent experiments). *, $P < 0.05$. (F) *Ccl2* mRNA expression in WT and *Csf2rb*$^{-/-}$ Ly-$6C^{high}$ monocytes and macrophages in MI tissue 2 d after MI ($n = 9$–10 per group from at least three independent experiments). ***, $P < 0.001$. (G) Ly-$6C^{high}$ monocytes, macrophages, neutrophils, and fibroblasts were sorted from 2-d-old infarct of WT or *Csf2rb*$^{-/-}$ mice and cultured in the presence or absence of GM-CSF for 48 h. GM-CSF protein levels were measured in the supernatants. Values are normalized to WT with medium ($n = 5$–6 per group from two independent experiments). **, $P < 0.01$. (H) Representative flow cytometric histograms for pSTAT5 expression in the indicated cells. Single cell suspension from hearts 2 d after MI was incubated with or without GM-CSF and stained with pSTAT5. (I) Illustration of experimental approach with adoptive transfer of sorted GFP^+ BM Ly-$6C^{high}$ monocytes (3×10^6) into WT or *Csf2*$^{-/-}$ mice 3 d after permanent coronary ligation. (J) Representative flow dot plots of infarcted hearts of WT and *Csf2*$^{-/-}$ mice for GFP^+ cells 3 h after the transfer. Quantification of GFP^+ cells in the hearts of indicated animals is also shown ($n = 4$ per group from two independent experiments). *, $P < 0.05$. For statistical analysis, two-tailed unpaired *t* test was performed to compare two groups, and one-way ANOVA followed by Tukey's test was performed for multiple comparisons. Results are shown as mean ± SEM.

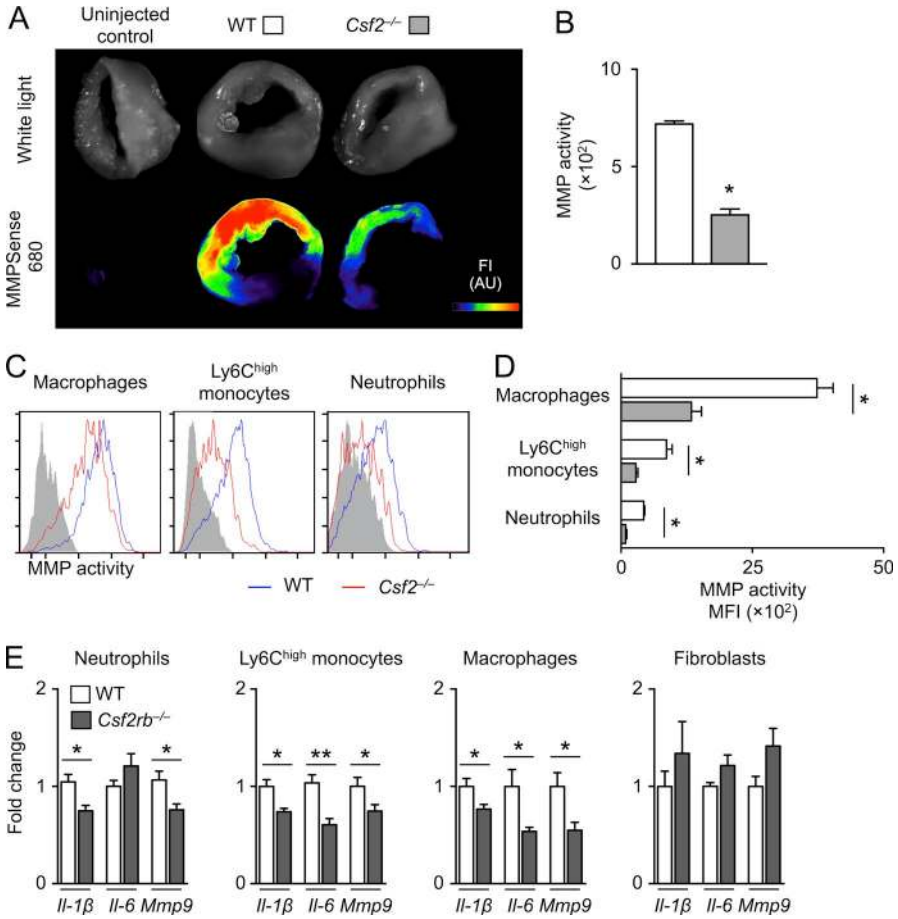

Figure 5. **GM-CSF promotes accumulation of proteolytic and inflammatory neutrophils and monocytes.** (A) Representative pictures of ex vivo fluorescence reflectance imaging using MMPSense 680 for WT and *Csf2*$^{-/-}$ infarcted hearts 3 d after MI. FI, fluorescent intensity. (B) Quantification of MMP activity in 3-d-old infarcts of WT and *Csf2*$^{-/-}$ mice (n = 4–6 per group). *, P < 0.05. (C) Representative flow cytometric histograms for MMP activity in macrophages, Ly-6C^{high} monocytes, and neutrophils. (D) Flow cytometry–based quantification of MMP activity (n = 4–6 per group). *, P < 0.05. (E) Gene expression levels of *Il-1β*, *Il-6*, and *Mmp9* in neutrophils, Ly-6C^{high} monocytes, macrophages, and fibroblasts sorted from WT and *Csf2rb*$^{-/-}$ MI tissue 3 d after MI (n = 5–12 per group from three independent experiments). *, P < 0.05; **, P < 0.01. For statistical analysis, two-tailed unpaired t test was performed to compare two groups. Results are shown as mean ± SEM.

2010). The BM, and to a lesser extent the spleen, manufactures neutrophils and monocytes through myelopoiesis, and although billions of cells are made every day in the steady state, output rises in response to injury or infection. Given leukocytes' central role in post-MI inflammation and repair, identifying signals that contribute to increased cell production has high importance.

Our study's findings, that GM-CSF controls neutrophil and monocyte production by acting on a specific BM progenitor, have several implications that extend beyond MI. Unlike M-CSF, the related growth factor that controls myeloid cell production in the steady state, GM-CSF contributes little to homeostatic hematopoiesis; mice lacking GM-CSF or its receptor have normal leukocyte levels and, aside from developing alveolar proteinosis as a result of defective surfactant clearance, have no demonstrable abnormalities. That said, accumulating evidence shows that the growth factor propels the inflammatory cascade. Our data contribute to this concept by demonstrating that GM-CSF–dependent leukocytosis relies not so much on a general increase in cell production as on a specific GM-CSFR–expressing subset within the MPP3 progenitor (Pietras et al., 2015). The BM, it seems, remains poised in a state of alert for GM-CSF should a need for increased cell production arise.

Once generated and released into the bloodstream, leukocytes follow chemotactic cues to find their destination tissue. Among the signals, the ischemic heart produces the chemokines Ccl2 (Hayashidani et al., 2003; Dewald et al., 2005), which attracts Ccr2^{+} monocytes, and Cxcl2, which attracts neutrophils (Soehnlein and Lindbom, 2010). We discovered that GM-CSF stimulates substantial Ccl2 and Cxcl2 in the heart after ischemic injury. Though many cells produce Ccl2 and Cxcl2, Ly-6C^{high} monocytes and macrophages are among the most abundant contributors of Ccl2, whereas neutrophils themselves produce Cxcl2. This provides for a parallel, feed-forward response that ensures massive monocyte and neutrophil accumulation over a short period of time (Fig. 9). Although they are required for wound healing, an overabundance of these cells results in excessive inflammation and proteolysis, which eventually leads to heart failure and death.

Our previous studies in sepsis, pneumonia, and atherosclerosis identified a B cell subset, which we called innate response activator, as a major GM-CSF source (Rauch et al., 2012; Hilgendorf et al., 2014b; Weber et al., 2014). This study identified no GM-CSF–producing B cells in the heart or spleen. However, the observation that cardiac fibroblasts make GM-CSF is intriguing, as fibroblasts also produce GM-CSF in other heart-related inflammatory dis-

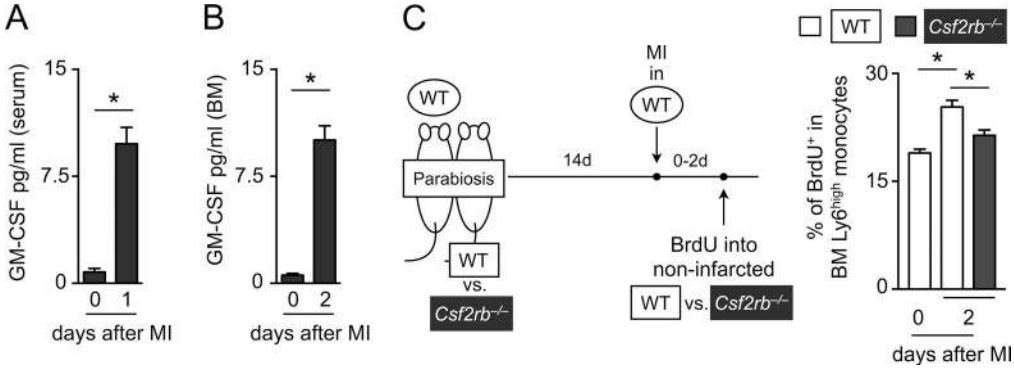

Figure 6. **Infarct-derived GM-CSF stimulates BM cell proliferation via circulation.** (A and B) GM-CSF protein levels in serum (A) and BM (B) at indicated time points after MI (n = 4 per group from two independent experiments). *, P < 0.05. (C) Diagram of the experimental design and quantification of percentage of BrdU$^+$ BM Ly-6C^{high} monocytes in the indicated noninfarcted parabionts before and 2 d after MI. 14 d after parabiosis surgery, MI was induced in WT mice (circle). Noninfarcted mice (WT or *Csf2rb*$^{-/-}$ mice with square) were analyzed 2 d post-MI. BrdU was injected into noninfarcted mice 2 h before death (n = 4–5 per group from at least two independent experiments). *, P < 0.05. For statistical analysis, two-tailed unpaired t test was performed to compare two groups, and one-way ANOVA followed by Tukey's test was performed for multiple comparisons. Results are shown as mean ± SEM.

eases, such as autoimmune myocarditis and Kawasaki disease (Wu et al., 2014; Stock et al., 2016). As nonhematopoietic cells, fibroblasts are strategically located to sense the cardiac microenvironment. During MI, when dying cardiomyocytes release danger-associated molecular patterns (Mann, 2015; Prabhu and Frangogiannis, 2016), cardiac fibroblasts can easily respond as they bear TLRs and other scavenger receptors. Our data accordingly indicate that multiple signals converging on the adapter molecules MyD88 or TRIF trigger GM-CSF production in the infarcted heart, which helps to generate and recruit hematopoietic cells that fuel inflammation. Experiments involving chimeras lacking the GM-CSF receptor underscore the importance of GM-CSF's action on the hematopoietic rather than the stromal compartments because left ventricular rupture ultimately depends on this dyad. This result should not be surprising given that inflammatory leukocytes are major sources of oxidases, proteases, and other factors that can antagonize the formation of a durable scar.

Drugs targeting GM-CSF or its receptor are available for human use, and several clinical trials are underway testing the efficacy of anti–GM-CSF therapy in various inflammatory diseases (Hamilton et al., 2016; Wicks and Roberts, 2016). As a mediator that governs production, recruitment, and function of myeloid cells after MI, GM-CSF should be considered a potential therapeutic target to foster salutary healing of the ischemic myocardium and prevent ischemic cardiomyopathy.

MATERIALS AND METHODS

Animals

C57BL/6 (WT), B6.SJL-Ptprc^{a}Pepc^b/BoyJ, C57BL/6-Tg(UBC-GFP)30Scha/J (GFP$^+$), B6.129P2(SJL)-Myd88$^{tm1.1Defr}$/J, B6.129-Tlr2^{tm1Kir}/J, B6(Cg)-Tlr4$^{tm1.2Karp}$/J, B6.129S1-Tlr7^{tm1Flv}/J, C57BL/6J-Tlr9^{M7Btlr}/Mmjax, B6.129S7-Il1r1$^{tm1/mx}$/J, C57BL/6J-Ticam1^{Lps2}/J, B6.Cg-Ccl2$^{tm1.1Pame}$/J, and B6.129S4-Ccr2^{tm1Ifc}/J (The Jackson Laboratory) were used in this study. *Csf2*$^{-/-}$ and *Csf2rb*$^{-/-}$ mice on C57BL/6 background (10 generations) were bred in-house (Rauch et al., 2012; Hilgendorf et al., 2014b; Weber et al., 2014). All experiments were conducted with male mice aged 8–16 wk at the time of death. All protocols were approved by the Animal Review Committee at Massachusetts General Hospital.

Animal models and in vivo interventions

Myocardial infarction. MI was induced by permanent ligation of the left anterior descending coronary artery (LAD) as previously described (Nahrendorf et al., 2007; Hilgendorf et al., 2014a). In brief, mice were anesthetized with isoflurane (2%/2 liters O_2), intubated, and ventilated with an Inspira Advanced Safety Single Animal Pressure/Volume Controlled Ventilator (Harvard Apparatus). Left thoracotomy was performed in the fourth intercostal space after shaving the chest wall. The left ventricle was visualized, and the LAD was ligated with monofilament 8-0 suture (Ethicon). The chest and skin were closed with a 7-0 nylon suture followed by removal of air from the thorax via a pleural catheter. The procedure was performed by the same surgeon blinded to genotypes.

BM transplantation. Naive C57BL/6 or *Csf2rb*$^{-/-}$ mice were lethally irradiated (950 cGy) and reconstituted with either WT or *Csf2rb*$^{-/-}$ BM cells to generate three groups: (a) WT^{WT} (irradiated WT mice reconstituted with WT BM), (b) WT$^{Csf2rb-/-}$ (irradiated WT mice reconstituted with *Csf2rb*$^{-/-}$ BM), and (c) *Csf2rb*$^{-/-WT}$ (irradiated *Csf2rb*$^{-/-}$ mice reconstituted with WT BM). After 7–8 wk to allow reconstitution, the mice were subjected to MI surgery.

Adoptive transfer. BM Ly-6C^{high} monocytes were collected from C57BL/6-Tg(UBC-GFP)30Scha/J mice by flow-

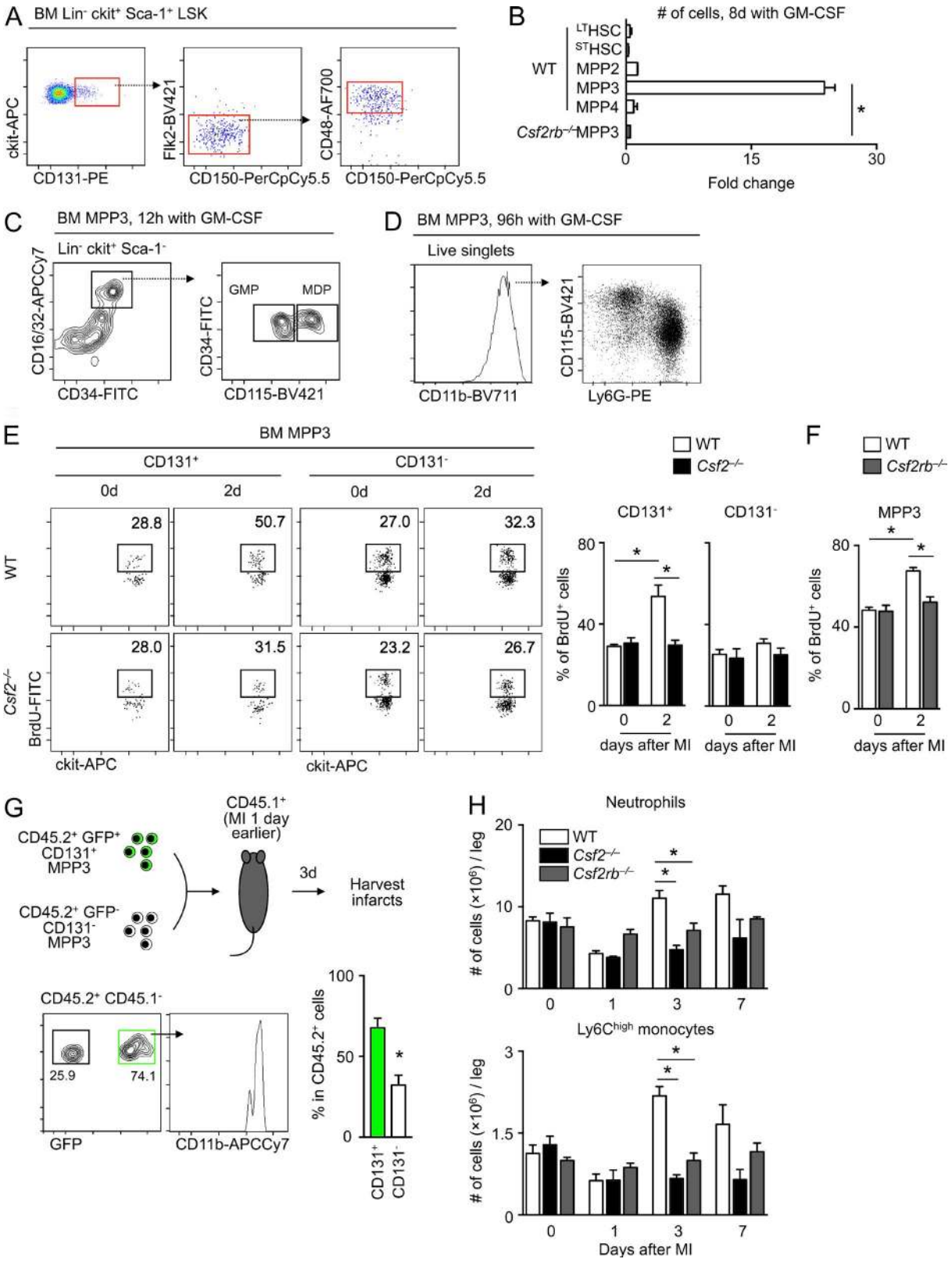

Figure 7. **CD131⁺ multipotent progenitor subset contributes to BM hematopoiesis in response to GM-CSF after MI.** (A) Representative flow dot plots for CD131⁺ cells in BM LSK. (B) Cell numbers of sorted LSK subpopulations stimulated with GM-CSF for 8 d. The data were normalized by 5×10^3 that were initially seeded into the culture plate (n = 3–4 per group from two to three independent experiments). *, $P < 0.05$. (C and D)

assisted cell sorting after enrichment of cells negative for CD3, CD19, B220, NK1.1, and Ly6G using magnetic cell separation. At 3 d after MI, 3×10^6 GFP$^+$ Ly-6C^{high} monocytes were injected intravenously into WT or *Csf2*$^{-/-}$ mice. For BM MPP3 transfer, CD131$^+$ MPP3s were sorted from C57BL/6-Tg(UBC-GFP)30Scha/J mice (CD45.2$^+$ GFP$^+$), and CD131$^-$ MPP3s were sorted from C57BL/6 mice (CD45.2$^+$ GFP$^-$). Those cells were intravenously injected at a 1:1 ratio (10^4 cells each) into B6.SJL-Ptprc^{a}Pepc^b/BoyJ (CD45.1$^+$) mice subjected to MI 1 d earlier.

Parabiosis. Parabiosis surgery was performed as previously described (Robbins et al., 2013). In brief, after shaving the corresponding lateral aspects of each mouse, matching skin incisions were made from behind the ear to the tail of each mouse, and the subcutaneous fascia was bluntly dissected to create 0.5 cm of free skin. The scapulae were sutured using mononylon 5.0 (Ethicon), and the dorsal and ventral skins were approximated by continuous suture. Mice were joined for 2 wk and then subjected to MI.

BrdU incorporation experiments. To assess cell proliferation, 1 mg BrdU was injected intraperitoneally 2 or 24 h before death and subsequent organ harvest. BrdU flow kit (BD Biosciences) was used to stain BrdU$^+$ cells.

Splenectomy. Splenectomy was performed as previously described (Swirski et al., 2009). In brief, during isoflurane anesthesia, the abdominal cavity of mice was opened, and the spleen vessels were cauterized. The spleen was carefully removed. For control experiments, the abdomen was opened, but the spleen was not excised.

Anti–GM-CSF neutralization antibody treatment. After coronary ligation, mice were randomly allocated to either anti–GM-CSF treatment or control IgG treatment groups. Neutralizing antibody against GM-CSF (MP1-22E9, eBioscience; 300 µg) or control IgG2a (eBR2a, eBioscience; 300 µg) was intravenously injected once a day for 3 d.

Recombinant mouse GM-CS injection. Recombinant mouse GM-CSF (BioLegend; 20 µg/kg) was intravenously injected into mice after the MI surgery twice a day for 3 d. PBS was used as a control.

Cardiac MRI

To assess cardiac function and morphology, MRI was performed on days 1 and 21 after MI as described previously (Sager et al., 2015). Cine images of the left ventricular short axis were obtained by using a 7-Tesla horizontal bore Pharmascan (Bruker) and a custom-built mouse cardiac coil (Rapid Biomedical). Left ventricular volume, ejection fraction, and infarct size were acquired and calculated as previously described.

Ex vivo fluorescence reflectance imaging

2 nmol of an MMP sensor (MMPSense-680; PerkinElmer) was intravenously injected into mice subjected to MI 2 d earlier. 24 h later, hearts were excised, and ex vivo fluorescence imaging was performed to interrogate magnitude and quality of MMP activity.

Cell isolation

Peripheral blood was collected by retroorbital bleeding, and erythrocytes were lysed in RBC lysis buffer (BioLegend). Spleens, femurs, tibias, and hearts were excised after vascular perfusion with cold PBS. Minced spleen and flushed BM were strained through 40-µm nylon mesh (BD Biosciences). Spleen cell suspensions were further subjected to RBC lysis. The naive hearts or infarcted areas with the border zone were minced and digested with 450 U/ml collagenase I, 125 U/ml collagenase XI, 60 U/ml DNase I, and 60 U/ml hyaluronidase (Sigma-Aldrich) in PBS for 1 h at 37°C with shaking. Total viable cell numbers were counted using Trypan blue (Cellgro, Mediatech).

Cell sorting. Single-cell suspensions of heart tissue and BM from indicated animals were made and stained to identify indicated cell populations. Cells were sorted on a FACS Aria II (BD Biosciences) directly into either RLT buffer for subsequent RNA isolation or complete medium for cell culture experiments.

Flow cytometry

Single-cell suspensions were stained in PBS supplemented with sterile 2% FBS and 0.5% BSA. The following monoclonal antibodies were used for flow cytometric analysis: anti-CD45 (30-F11), anti-CD45.1 (clone A20), anti-CD45.2 (clone 104), anti-CD3e (clone 145-2C11), anti-CD90.2 (clone 53–2.1), anti-CD19 (clone 6D5), anti-B220 (clone

Representative flow cytometric plots 12 h (C) and 96 h (D) after placement of sorted BM MPP3s in medium containing GM-CSF. (E) Representative flow dot plots and quantification of BrdU$^+$ CD131$^+$ or CD131$^-$ MPP3s in WT and *Csf2*$^{-/-}$ mice at indicated time points (n = 5–6 per group from three independent experiments). BrdU was injected 24 h before death. *, $P < 0.05$. (F) Quantification of BrdU$^+$ MPP3s in WT and *Csf2rb*$^{-/-}$ mice before and 2 d after MI (n = 5–6 per group from three independent experiments). BrdU was injected 24 h before death. *, $P < 0.05$. (G) Illustration of experimental setup and flow dot plots of CD45.2$^+$ cells in infarcted myocardium with quantification. Injected CD45.2$^+$ CD131$^+$ MPP3s are detected as GFP$^+$, whereas CD45.2$^+$ CD131$^-$ MPP3s are shown as GFP$^-$ (n = 4–5 per group from two independent experiments). *, $P < 0.05$. (H) Time course of BM neutrophil and Ly-6C^{high} monocyte numbers in WT, *Csf2*$^{-/-}$, and *Csf2rb*$^{-/-}$ mice after MI (n = 4–7 per group from at least three independent experiments). *, $P < 0.05$. For statistical analysis, two-tailed unpaired t test was performed to compare two groups, and one-way ANOVA followed by Tukey's test was performed for multiple comparisons. Results are shown as mean ± SEM.

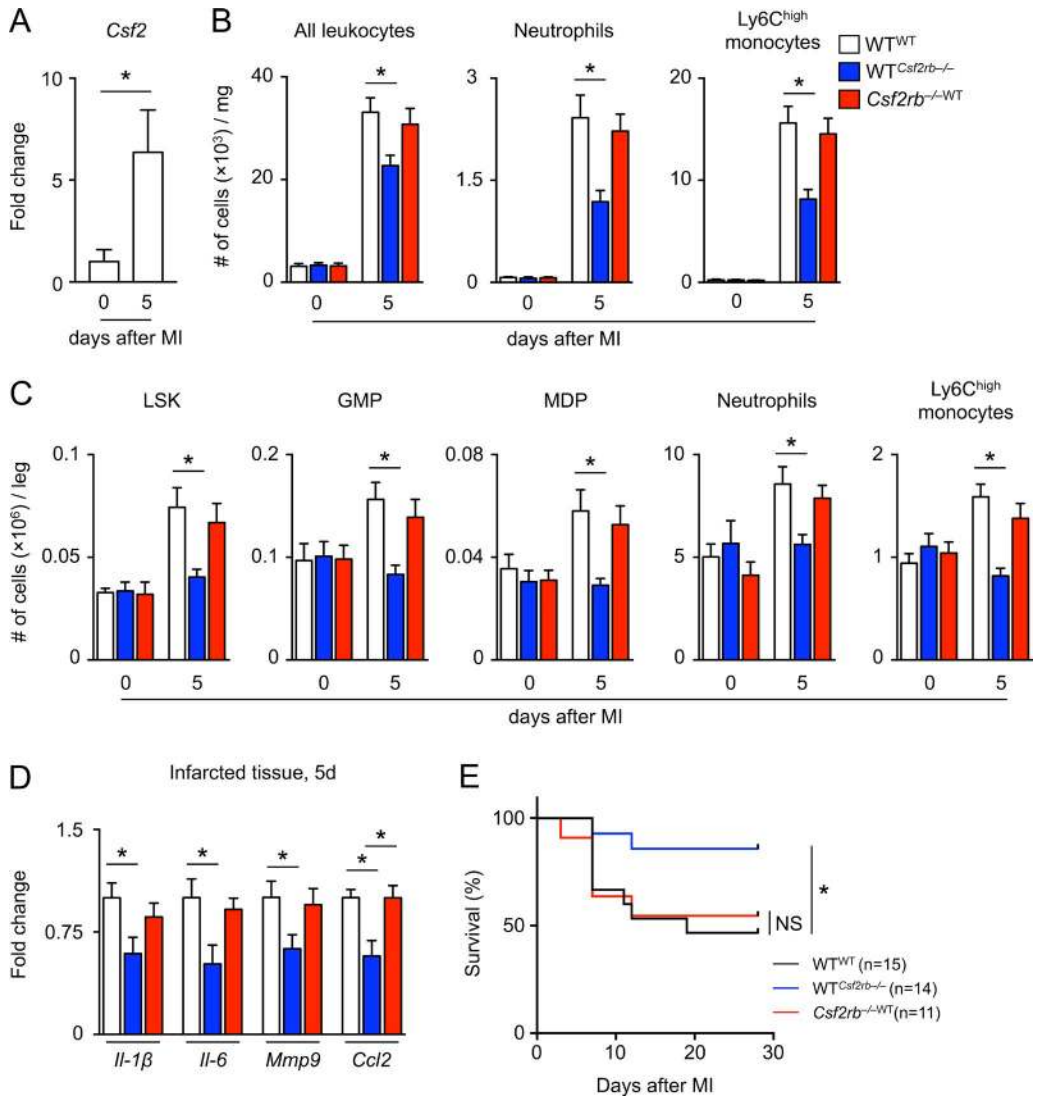

Figure 8. **GM-CSF licenses BM-derived cells to cause left ventricular rupture and immunopathology after coronary artery ligation.** WT mice were lethally irradiated and reconstituted with BM cells from either WT or *Csf2rb*$^{-/-}$ mice (WT^{WT} and WT$^{Csf2rb-/-}$ mice, respectively). *Csf2rb*$^{-/-WT}$ mice were made by reconstitution of irradiated *Csf2rb*$^{-/-}$ mice with WT BM. (A) *Csf2* mRNA expression levels in infarcted tissue of WT^{WT} mice before and 5 d after MI (n = 3–6 per group from two independent experiments). *, P < 0.05. (B) Flow cytometry–based quantification of indicated cells in the hearts of WT^{WT}, WT$^{Csf2rb-/-}$, and *Csf2rb*$^{-/-WT}$ mice before and 5 d after MI (n = 4–7 per group from at least two independent experiments). *, P < 0.05. (C) Quantification of indicated BM cell fractions of WT^{WT}, WT$^{Csf2rb-/-}$, and *Csf2rb*$^{-/-WT}$ mice before and 5 d after MI (n = 4–7 per group from at least two independent experiments). *, P < 0.05. (D) mRNA expression levels of *Il-1β*, *Il-6*, *Mmp9*, and *Ccl2* in infarcted tissue of WT^{WT}, WT$^{Csf2rb-/-}$, and *Csf2rb*$^{-/-WT}$ mice 5 d after MI (n = 6–8 per group from at least two independent experiments). *, P < 0.05. (E) Post-MI survival rate after MI in WT^{WT}, WT$^{Csf2rb-/-}$, and *Csf2rb*$^{-/-WT}$ mice. Data are from three independent experiments. *, P < 0.05. For statistical analysis, log-rank test was applied to compare survival curves, two-tailed unpaired t test was performed to compare two groups, and one-way ANOVA followed by Tukey's test was performed for multiple comparisons. Results are shown as mean ± SEM.

RA3-6B2), anti-NK1.1 (clone PK136), anti-Ly6G (clone 1A8), anti–Ly-6C (AL-21), anti-MHCII (clone AF6-120.1), anti-F4/80 (clone BM8), anti-CD11b (clone M1/70,), anti-CD11c (clone HL3), anti-CD115 (clone AFS98), anti-Ter119 (clone Ter-119), anti-CD34 (clone RAM34), anti-flk2 (clone A2F10), anti-CD150 (clone TC15-12F12.2), anti-Sca1 (clone D7), anti–c-kit (clone 2B8), anti-CD48 (clone HM48-1), anti-CD16/32 (clone 93), anti-Gr1 (clone RB6-8C5), anti-CD127 (clone A7R34), anti-CD131 (clone REA193), anti-CD31 (clone 390), anti-MEFSK4 (clone mEF-SK4), anti-CCR2 (clone 475301), anti-CXCR2 (clone TG11/CXCR2), anti–activated caspase 3 (clone C92-605), pSTAT5 (clone pY694), and isotype controls. Antibodies were purchased from BioLegend, BD Biosciences, eBioscience, or Miltenyi Biotec. Viable cells were identified as unstained with Zombie Aqua (BioLegend).

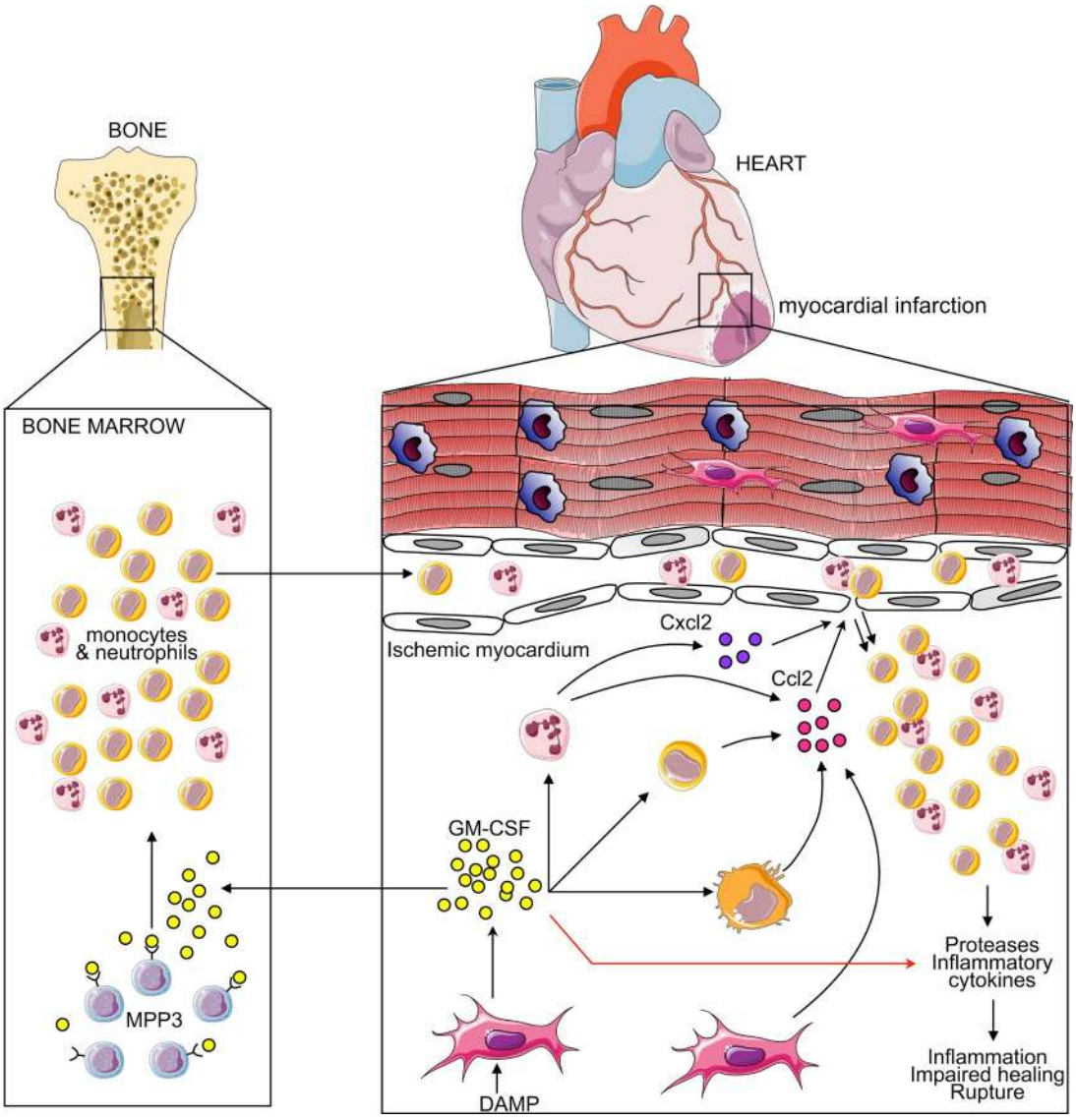

Figure 9. **Proposed model.** The cartoon depicts functions by which GM-CSF aggravates healing after MI. GM-CSF is produced by cardiac fibroblasts in response to damage-associated molecular patterns (DAMP). Fibroblast-produced GM-CSF acts locally on myeloid cells, which promote chemokine-dependent leukocyte recruitment. Fibroblast-generated GM-CSF also acts at a distance in the BM, where it stimulates CD131$^+$ MPP3 to produce proteolytic and inflammatory neutrophils and monocytes. Together, these local and systemic functions result in enhanced production and recruitment of cells that aggravate post-MI healing.

Staining strategies. For intracellular staining, cells were fixed and permeabilized with BD Cytofix/Cytoperm (BD Biosciences) according to the manufacturer's instructions. For pSTAT5 staining, cells were stimulated with or without GM-CSF–containing medium (20 ng/ml) for 30 min at 37°C to induce phosphorylation of STAT5, followed by addition of 4% PFA solution (pH 7.4) to obtain a final concentration of 2%. After fixation for 20 min, cells were resuspended in 1 ml ice-cold methanol to permeabilize. After 30 min of incubation at 4°C, cells were washed twice and stained with anti-pSTAT5 antibody as well as antibodies for extracellular antigens for 45 min at room temperature before a final wash and acquisition. Specifically, cardiac cells were defined as (1) Ly-6C^{high} monocytes (CD45$^+$Lin$^-$CD11b$^+$F4/80$^-$Ly-6C^{high}), (2) neutrophils (CD45$^+$CD11b$^+$Lin$^+$F4/80$^-$), (3) macrophages (CD45$^+$Lin$^-$CD11b$^+$F4/80$^+$Ly-6C^{low}), (4) endothelial cells (CD45$^-$CD31$^+$MEFSK4$^-$), (5) fibroblasts (CD45$^-$CD31$^-$MEFSK4$^+$), and (6) other stromal cells (CD45$^-$CD31$^-$MEFSK4$^-$). BM cells were defined as (1) monocytes (CD45$^+$Lin$^-$CD11b$^+$CD115$^+$F4/80$^-$), (2) neutrophils (CD45$^+$Ly6G$^+$CD11b$^+$CD115$^-$F4/80$^-$MHCII$^-$), (3) ^{LT}HSC (Lin$_2^-$ckit$^+$Sca1$^+$flk2$^-$CD48$^-$CD150$^+$), (4) STHSC (Lin$_2^-$ckit$^+$Sca1$^+$flk2$^-$CD48$^-$

$CD150^-$), (5) MPP2 ($Lin_2^-ckit^+Sca1^+flk2^-CD48^+CD150^+$), (6) MPP3 ($Lin_2^-ckit^+Sca1^+flk2^-CD48^+CD150^-$), (7) MPP4 ($Lin_2^-ckit^+Sca1^+flk2^+CD150^-$), (8) GMP ($Lin_2^-ckit^+Sca1^-CD34^+CD16/32^{high}CD115^-$), and (9) MDP ($Lin_2^-ckit^+Sca1^-CD34^+CD16/32^{high}CD115^+$). Lineages were defined as Lin: CD3, CD90.2, CD19, B220, NK1.1, Ter119, Ly6G; Lin_2: CD3, CD90.2, CD19, B220, NK1.1, Ter119, Gr1, CD127, CD11c. Data were acquired on a LSRII and analyzed with FlowJo (Tree Star).

Cell culture

For all cell culture experiments, cells were cultured in complete medium (RPMI-1640 supplemented with 10% FBS, 2 mM L-glutamine, 100 U/ml penicillin and streptomycin, 10 mM Hepes, 50 µM 2-mercaptoethanol, 1 mM sodium pyruvate, and 1× nonessential amino acids), and kept in a humidified 5% CO_2 incubator at 37°C. To determine the effect of GM-CSF on CCL2 production, neutrophils, Ly-$6C^{high}$ monocytes, macrophages, and fibroblasts were sorted from WT and *Csf2rb*$^{-/-}$ mice on the FACS Aria II, and 5×10^3 cells were seeded into 96-well plates in 200 µl medium. After incubation with or without GM-CSF for 48 h, supernatants were collected, and CCL2 levels were measured by ELISA. To identify the cellular target of GM-CSF in BM LSK compartment, 5×10^3 sorted ^{LT}HSC, STHSC, MPP2, MPP3, and MPP4 cells were cultured with and without GM-CSF for indicated periods, followed by counting and staining after retrieval from the 96-well plates. To determine the effect of danger signals on GM-CSF production in cardiac fibroblasts after MI, 3×10^4 cardiac fibroblasts sorted from 1-d-old infarct were plated onto 96-well plates in 200 µl medium and incubated in the presence or absence of poly(I:C) or CpG (InvivoGen) for 48 h. Supernatants were collected, and GM-CSF levels were measured by ELISA.

Reverse transcriptional PCR

Tissue. Total RNA was isolated using the RNeasy Mini kit (Qiagen) according to the manufacturer's instructions. cDNA was generated from 1 µg total RNA per sample using High Capacity cDNA Reverse Transcription kit (Applied Biosystems).

Cells. 2×10^4 total leukocytes, neutrophils, Ly-$6C^{high}$ monocytes, macrophages, endothelial cells, fibroblasts, and other stromal cells were sorted from infarcted myocardium, and total RNA was extracted using the RNeasy Micro kit (Qiagen) followed by cDNA transcription. Quantitative real-time TaqMan PCR was performed using the following TaqMan primers (Applied Biosystems): Il-1β (Mm01336189_m1), Il-3 (Mm00439631_m1), Il-5 (Mm00439646_m1), Il-6 (Mm00446190_m1), Mmp9 (Mm00442991_m1), Col1a1 (Mm00801666_g1), Pdgfra (Mm00440701_m1), Postn (Mm01284919_m1), Csf2 (Mm01290062_m1), Cxcl1 (Mm04207460_m1), Cxcl2 (Mm00436450_m1), Ccl2 (Mm00441242_m1), Ccl3 (Mm00441259_g1), Ccl5 (Mm01302427_m1), Ccl7 (Mm00443113_m1), Cx3cl1 (Mm00436454_m1), Ccl2 (Mm00441242_m1), Myh6 (Mm00440359_m1), Il-23a (Mm00518984_m1), and housekeeping gene Gapdh (Mm99999915_g1). PCR was run on a 7500 thermal cycler (Applied Biosystems), and data were quantified with the $2^{-\Delta Ct}$ method.

Histological methods

Hearts from WT and *Csf2*$^{-/-}$ mice (7 d after MI) were embedded in Tissue-Tek OCT compound (Sakura Finetek), frozen in 2-methylbutane (Thermo Fisher Scientific) cooled with dry ice, and sectioned into 6-µm slices. Immunohistochemistry was performed using antibodies against CD11b (dilution 1:25, clone M1/70; BD Biosciences), collagen 1 (dilution 1:50, ab21286; Abcam), CD31 (dilution 1:5, clone MEC13.3; BD Biosciences), and α-smooth muscle actin (dilution 1:50, ab5694; Abcam). Biotinylated rabbit anti–rat IgG (dilution 1:100, BA4001) or biotinylated goat anti–rabbit IgG (dilution 1:100, BA1000) followed by Vectastain Elite ABC HRP kit (PK-6100; all from Vector Laboratories) were applied to the sections, and AEC substrate chromogen (K3464; Dako/Agilent) was used for color development. Human heart samples were obtained from autopsies performed in the Department of Pathology, Massachusetts General Hospital. The study was approved by the Human Subjects Institutional Review Board at Massachusetts General Hospital. Hearts from two patients who died within 2 d after MI (acute infarct), two patients who died 7 d after MI (late infarct), and two patients who died from other reasons outside the heart were used in this study. Samples were fixed in 10% formalin and embedded in paraffin for histological sectioning (4-µm-thick slices). After deparaffinization and heat-induced antigen retrieval, sections were blocked with 4% normal goat serum for 45 min and stained with rabbit anti–human C4d (dilution 1:50, 12-5000; American Research Products). For immunofluorescence staining, rabbit anti–human GM-CSF (dilution 1:100, bs-3790R, Bioss) and guinea pig anti–human vimentin (dilution 1:50, GP53; Progen) were incubated at 4°C overnight, followed by secondary antibodies, DyLight680 goat anti–rabbit IgG (dilution 1:100, 35568; Thermo Fisher Scientific) and biotinylated anti–guinea pig IgG (dilution 1:100, BA7000, Vector Laboratories). To detect vimentin, streptavidin Dylight594 (dilution 1:600, SA-5594; Vector Laboratories) was applied, and nuclei were counterstained by DAPI (D12490; Thermo Fisher Scientific). Images were captured by using a BX63 automated fluorescence microscope (Olympus).

ELISA

GM-CSF levels were measured in heart homogenates, serum, and BM fluids with the Mouse GM-CSF ELISA kit (R&D Systems). CCL2/MCP-1 levels were measured in cell culture supernatants with the CCL2 ELISA kit (R&D Systems) according to the manufacturer's instructions.

Statistics

Results are shown as mean ± SEM. Statistical tests included unpaired, two-tailed nonparametric Mann–Whitney tests

(when Gaussian distribution was not assumed) or unpaired, two-tailed parametric *t* tests with Welch's correction (when Gaussian distribution was assumed). For multiple comparisons, nonparametric multiple comparisons test comparing mean rank of each group (when Gaussian distribution was not assumed) or one-way ANOVA followed by Tukey's test were performed. Survival distributions were estimated by the Kaplan–Meier method and compared by the log-rank test. P values of 0.05 or less were considered to denote significance.

Online supplemental material

Fig. S1 shows additional readouts from MRI and cell quantification. Fig. S2 shows gating strategies for HSPCs. Fig. S3 shows experiments using splenectomy.

ACKNOWLEDGMENTS

This work was supported in part by National Institutes of Health grants R35HL135752, R01 HL095612, and R01 HL128264; the American Heart Association's Established Investigator Award; and the Patricia and Scott Eston MGH Research Scholar (to F.K. Swirski). A. Anzai was supported by grants from the Banyu Life Science Foundation International. J.E. Mindur was supported by a National Institutes of Health Ruth L. Kirschstein Institutional National Research Service Award training grant (T32 AI118692). M. Nairz was supported by an Austrian Science Fund (FWF) Erwin Schroedinger Fellowship (J3486-B13). P. Libby was supported by National Institutes of Health grant R01 HL080472 and the Robert R. McCormick Foundation Charitable Fund.

The authors declare no competing financial interests.

Author contributions: A. Anzai conceived the project, designed and performed experiments, analyzed and interpreted data, and wrote the manuscript; J. Choi, S. He, A.M. Fenn, M. Nairz, S. Rattik, C. McAlpine, J.E. Mindur, C. Chan, Y. Iwamoto, B. Tricot, and G.R. Wojtkiewicz performed experiments; R. Weissleder, P. Libby, and B. Becher provided intellectual input and edited the manuscript; M. Nahrendorf provided intellectual input, designed experiments, and edited the manuscript. J.R. Stone provided materials and edited the manuscript; and F.K. Swirski conceived the project, designed experiments, analyzed and interpreted data, and wrote the manuscript.

Submitted: 13 April 2017
Revised: 2 August 2017
Accepted: 28 August 2017

REFERENCES

Anzai, A., T. Anzai, S. Nagai, Y. Maekawa, K. Naito, H. Kaneko, Y. Sugano, T. Takahashi, H. Abe, S. Mochizuki, et al. 2012. Regulatory role of dendritic cells in postinfarction healing and left ventricular remodeling. *Circulation*. 125:1234–1245. https://doi.org/10.1161/CIRCULATIONAHA.111.052126

Becher, B., S. Tugues, and M. Greter. 2016. GM-CSF: From Growth Factor to Central Mediator of Tissue Inflammation. *Immunity.* 45:963–973. https://doi.org/10.1016/j.immuni.2016.10.026

Bradley, T.R., and D. Metcalf. 1966. The growth of mouse bone marrow cells in vitro. *Aust. J. Exp. Biol. Med. Sci.* 44:287–300. https://doi.org/10.1038/icb.1966.28

Brown, D.W., W.H. Giles, and J.B. Croft. 2001. White blood cell count: an independent predictor of coronary heart disease mortality among a national cohort. *J. Clin. Epidemiol.* 54:316–322. https://doi.org/10.1016/S0895-4356(00)00296-1

Bruno, S., B. Bussolati, P. Scacciatella, S. Marra, F. Sanavio, C. Tarella, and G. Camussi. 2006. Combined administration of G-CSF and GM-CSF stimulates monocyte-derived pro-angiogenic cells in patients with acute myocardial infarction. *Cytokine.* 34:56–65. https://doi.org/10.1016/j.cyto.2006.03.014

Dewald, O., P. Zymek, K. Winkelmann, A. Koerting, G. Ren, T. Abou-Khamis, L.H. Michael, B.J. Rollins, M.L. Entman, and N.G. Frangogiannis. 2005. CCL2/Monocyte Chemoattractant Protein-1 regulates inflammatory responses critical to healing myocardial infarcts. *Circ. Res.* 96:881–889. https://doi.org/10.1161/01.RES.0000163017.13772.3a

Dutta, P., G. Courties, Y. Wei, F. Leuschner, R. Gorbatov, C.S. Robbins, Y. Iwamoto, B. Thompson, A.L. Carlson, T. Heidt, et al. 2012. Myocardial infarction accelerates atherosclerosis. *Nature.* 487:325–329. https://doi.org/10.1038/nature11260

Hajj-Ali, R., W. Zareba, R. Ezzeddine, and A.J. Moss. 2001. Relation of the leukocyte count to recurrent cardiac events in stable patients after acute myocardial infarction. *Am. J. Cardiol.* 88:1221–1224. https://doi.org/10.1016/S0002-9149(01)02080-X

Hamilton, J.A. 2008. Colony-stimulating factors in inflammation and autoimmunity. *Nat. Rev. Immunol.* 8:533–544. https://doi.org/10.1038/nri2356

Hamilton, J.A., A.D. Cook, and P.P. Tak. 2016. Anti-colony-stimulating factor therapies for inflammatory and autoimmune diseases. *Nat. Rev. Drug Discov.* 16:53–70. https://doi.org/10.1038/nrd.2016.231

Hayashidani, S., H. Tsutsui, T. Shiomi, M. Ikeuchi, H. Matsusaka, N. Suematsu, J. Wen, K. Egashira, and A. Takeshita. 2003. Anti-monocyte chemoattractant protein-1 gene therapy attenuates left ventricular remodeling and failure after experimental myocardial infarction. *Circulation.* 108:2134–2140. https://doi.org/10.1161/01.CIR.0000092890.29552.22

Heidt, T., G. Courties, P. Dutta, H.B. Sager, M. Sebas, Y. Iwamoto, Y. Sun, N. Da Silva, P. Panizzi, A.M. van der Laan, et al. 2014. Differential contribution of monocytes to heart macrophages in steady-state and after myocardial infarction. *Circ. Res.* 115:284–295. https://doi.org/10.1161/CIRCRESAHA.115.303567

Heymans, S., A. Luttun, D. Nuyens, G. Theilmeier, E. Creemers, L. Moons, G.D. Dyspersin, J.P. Cleutjens, M. Shipley, A. Angellilo, et al. 1999. Inhibition of plasminogen activators or matrix metalloproteinases prevents cardiac rupture but impairs therapeutic angiogenesis and causes cardiac failure. *Nat. Med.* 5:1135–1142. https://doi.org/10.1038/13459

Hilgendorf, I., L.M. Gerhardt, T.C. Tan, C. Winter, T.A. Holderried, B.G. Chousterman, Y. Iwamoto, R. Liao, A. Zirlik, M. Scherer-Crosbie, et al. 2014a. Ly-6Chigh monocytes depend on Nr4a1 to balance both inflammatory and reparative phases in the infarcted myocardium. *Circ. Res.* 114:1611–1622. https://doi.org/10.1161/CIRCRESAHA.114.303204

Hilgendorf, I., I. Theurl, L.M. Gerhardt, C.S. Robbins, G.F. Weber, A. Gonen, Y. Iwamoto, N. Degousee, T.A. Holderried, C. Winter, et al. 2014b. Innate response activator B cells aggravate atherosclerosis by stimulating T helper-1 adaptive immunity. *Circulation.* 129:1677–1687. https://doi.org/10.1161/CIRCULATIONAHA.113.006381

Kaikita, K., T. Hayasaki, T. Okuma, W.A. Kuziel, H. Ogawa, and M. Takeya. 2004. Targeted deletion of CC chemokine receptor 2 attenuates left ventricular remodeling after experimental myocardial infarction. *Am. J. Pathol.* 165:439–447. https://doi.org/10.1016/S0002-9440(10)63309-3

Kempf, T., A. Zarbock, C. Widera, S. Butz, A. Stadtmann, J. Rossaint, M. Bolomini-Vittori, M. Korf-Klingebiel, L.C. Napp, B. Hansen, et al. 2011. GDF-15 is an inhibitor of leukocyte integrin activation required for survival after myocardial infarction in mice. *Nat. Med.* 17:581–588. https://doi.org/10.1038/nm.2354

Kyne, L., J.M. Hausdorff, E. Knight, L. Dukas, G. Azhar, and J.Y. Wei. 2000. Neutrophilia and congestive heart failure after acute myocardial infarction. *Am. Heart J.* 139:94–100. https://doi.org/10.1016/S0002-8703(00)90314-4

Leuschner, F., P. Panizzi, I. Chico-Calero, W.W. Lee, T. Ueno, V. Cortez-Retamozo, P. Waterman, R. Gorbatov, B. Marinelli, Y. Iwamoto, et al.

2010. Angiotensin-converting enzyme inhibition prevents the release of monocytes from their splenic reservoir in mice with myocardial infarction. *Circ. Res.* 107:1364–1373. https://doi.org/10.1161/CIRCRESAHA.110.227454

Leuschner, F., P.J. Rauch, T. Ueno, R. Gorbatov, B. Marinelli, W.W. Lee, P. Dutta, Y. Wei, C. Robbins, Y. Iwamoto, et al. 2012. Rapid monocyte kinetics in acute myocardial infarction are sustained by extramedullary monocytopoiesis. *J. Exp. Med.* 209:123–137. https://doi.org/10.1084/jem.20111009

Madjid, M., I. Awan, J.T. Willerson, and S.W. Casscells. 2004. Leukocyte count and coronary heart disease: implications for risk assessment. *J. Am. Coll. Cardiol.* 44:1945–1956. https://doi.org/10.1016/j.jacc.2004.07.056

Maekawa, Y., T. Anzai, T. Yoshikawa, Y. Asakura, T. Takahashi, S. Ishikawa, H. Mitamura, and S. Ogawa. 2002. Prognostic significance of peripheral monocytosis after reperfused acute myocardial infarction:a possible role for left ventricular remodeling. *J. Am. Coll. Cardiol.* 39:241–246. https://doi.org/10.1016/S0735-1097(01)01721-1

Maekawa, Y., T. Anzai, T. Yoshikawa, Y. Sugano, K. Mahara, T. Kohno, T. Takahashi, and S. Ogawa. 2004. Effect of granulocyte-macrophage colony-stimulating factor inducer on left ventricular remodeling after acute myocardial infarction. *J. Am. Coll. Cardiol.* 44:1510–1520. https://doi.org/10.1016/j.jacc.2004.05.083

Mann, D.L. 2015. Innate immunity and the failing heart: the cytokine hypothesis revisited. *Circ. Res.* 116:1254–1268. https://doi.org/10.1161/CIRCRESAHA.116.302317

Matsumura, S., S. Iwanaga, S. Mochizuki, H. Okamoto, S. Ogawa, and Y. Okada. 2005. Targeted deletion or pharmacological inhibition of MMP-2 prevents cardiac rupture after myocardial infarction in mice. *J. Clin. Invest.* 115:599–609. https://doi.org/10.1172/JCI22304

Murphy, A.J., M. Akhtari, S. Tolani, T. Pagler, N. Bijl, C.L. Kuo, M. Wang, M. Sanson, S. Abramowicz, C. Welch, et al. 2011. ApoE regulates hematopoietic stem cell proliferation, monocytosis, and monocyte accumulation in atherosclerotic lesions in mice. *J. Clin. Invest.* 121:4138–4149. https://doi.org/10.1172/JCI57559

Nahrendorf, M., F.K. Swirski, E. Aikawa, L. Stangenberg, T. Wurdinger, J.L. Figueiredo, P. Libby, R. Weissleder, and M.J. Pittet. 2007. The healing myocardium sequentially mobilizes two monocyte subsets with divergent and complementary functions. *J. Exp. Med.* 204:3037–3047. https://doi.org/10.1084/jem.20070885

Nahrendorf, M., M.J. Pittet, and F.K. Swirski. 2010. Monocytes: protagonists of infarct inflammation and repair after myocardial infarction. *Circulation.* 121:2437–2445. https://doi.org/10.1161/CIRCULATIONAHA.109.916346

Panizzi, P., F.K. Swirski, J.L. Figueiredo, P. Waterman, D.E. Sosnovik, E. Aikawa, P. Libby, M. Pittet, R. Weissleder, and M. Nahrendorf. 2010. Impaired infarct healing in atherosclerotic mice with Ly-6C(hi) monocytosis. *J. Am. Coll. Cardiol.* 55:1629–1638. https://doi.org/10.1016/j.jacc.2009.08.089

Parissis, J.T., S. Adamopoulos, K.F. Venetsanou, D.G. Mentzikof, S.M. Karas, and D.T. Kremastinos. 2000. Clinical and neurohormonal correlates of circulating granulocyte-macrophage colony-stimulating factor in severe heart failure secondary to ischemic or idiopathic dilated cardiomyopathy. *Am. J. Cardiol.* 86:707–710. https://doi.org/10.1016/S0002-9149(00)01062-6

Parissis, J.T., S. Adamopoulos, K. Venetsanou, G. Kostakis, A. Rigas, S.M. Karas, and D. Kremastinos. 2004. Plasma profiles of circulating granulocyte-macrophage colony-stimulating factor and soluble cellular adhesion molecules in acute myocardial infarction. Contribution to post-infarction left ventricular dysfunction. *Eur. Cytokine Netw.* 15:139–144.

Pietras, E.M., D. Reynaud, Y.A. Kang, D. Carlin, F.J. Calero-Nieto, A.D. Leavitt, J.M. Stuart, B. Gottgens, and E. Passegue. 2015. Functionally Distinct Subsets of Lineage-Biased Multipotent Progenitors Control Blood Production in Normal and Regenerative Conditions. *Cell Stem Cell.* 17:35–46. https://doi.org/10.1016/j.stem.2015.05.003

Pinto, A.R., A. Ilinykh, M.J. Ivey, J.T. Kuwabara, M.L. D'Antoni, R. Debuque, A. Chandran, L. Wang, K. Arora, N.A. Rosenthal, and M.D. Tallquist. 2016. Revisiting Cardiac Cellular Composition. *Circ. Res.* 118:400–409. https://doi.org/10.1161/CIRCRESAHA.115.307778

Prabhu, S.D., and N.G. Frangogiannis. 2016. The Biological Basis for Cardiac Repair After Myocardial Infarction: From Inflammation to Fibrosis. *Circ. Res.* 119:91–112. https://doi.org/10.1161/CIRCRESAHA.116.303577

Rauch, P.J., A. Chudnovskiy, C.S. Robbins, G.F. Weber, M. Etzrodt, I. Hilgendorf, E. Tiglao, J.L. Figueiredo, Y. Iwamoto, I. Theurl, et al. 2012. Innate response activator B cells protect against microbial sepsis. *Science.* 335:597–601. https://doi.org/10.1126/science.1215173

Robbins, C.S., I. Hilgendorf, G.F. Weber, I. Theurl, Y. Iwamoto, J.L. Figueiredo, R. Gorbatov, G.K. Sukhova, L.M. Gerhardt, D. Smyth, et al. 2013. Local proliferation dominates lesional macrophage accumulation in atherosclerosis. *Nat. Med.* 19:1166–1172. https://doi.org/10.1038/nm.3258

Romson, J.L., B.G. Hook, S.L. Kunkel, G.D. Abrams, M.A. Schork, and B.R. Lucchesi. 1983. Reduction of the extent of ischemic myocardial injury by neutrophil depletion in the dog. *Circulation.* 67:1016–1023. https://doi.org/10.1161/01.CIR.67.5.1016

Sager, H.B., T. Heidt, M. Hulsmans, P. Dutta, G. Courties, M. Sebas, G.R. Wojtkiewicz, B. Tricot, Y. Iwamoto, Y. Sun, et al. 2015. Targeting Interleukin-1beta Reduces Leukocyte Production After Acute Myocardial Infarction. *Circulation.* 132:1880–1890. https://doi.org/10.1161/CIRCULATIONAHA.115.016160

Seiler, C., T. Pohl, K. Wustmann, D. Hutter, P.A. Nicolet, S. Windecker, F.R. Eberli, and B. Meier. 2001. Promotion of collateral growth by granulocyte-macrophage colony-stimulating factor in patients with coronary artery disease: a randomized, double-blind, placebo-controlled study. *Circulation.* 104:2012–2017. https://doi.org/10.1161/hc4201.097835

Soehnlein, O., and L. Lindbom. 2010. Phagocyte partnership during the onset and resolution of inflammation. *Nat. Rev. Immunol.* 10:427–439. https://doi.org/10.1038/nri2779

Stock, A.T., J.A. Hansen, M.A. Sleeman, B.S. McKenzie, and I.P. Wicks. 2016. GM-CSF primes cardiac inflammation in a mouse model of Kawasaki disease. *J. Exp. Med.* 213:1983–1998. https://doi.org/10.1084/jem.20151853

Subramanian, M., E. Thorp, and I. Tabas. 2015. Identification of a non-growth factor role for GM-CSF in advanced atherosclerosis: promotion of macrophage apoptosis and plaque necrosis through IL-23 signaling. *Circ. Res.* 116:e13–e24. https://doi.org/10.1161/CIRCRESAHA.116.304794

Swirski, F.K., and M. Nahrendorf. 2013. Leukocyte behavior in atherosclerosis, myocardial infarction, and heart failure. *Science.* 339:161–166. https://doi.org/10.1126/science.1230719

Swirski, F.K., P. Libby, E. Aikawa, P. Alcaide, F.W. Luscinskas, R. Weissleder, and M.J. Pittet. 2007. Ly-6Chi monocytes dominate hypercholesterolemia-associated monocytosis and give rise to macrophages in atheromata. *J. Clin. Invest.* 117:195–205. https://doi.org/10.1172/JCI29950

Swirski, F.K., M. Nahrendorf, M. Etzrodt, M. Wildgruber, V. Cortez-Retamozo, P. Panizzi, J.L. Figueiredo, R.H. Kohler, A. Chudnovskiy, P. Waterman, et al. 2009. Identification of splenic reservoir monocytes and their deployment to inflammatory sites. *Science.* 325:612–616. https://doi.org/10.1126/science.1175202

Theurl, I., I. Hilgendorf, M. Nairz, P. Tymoszuk, D. Haschka, M. Asshoff, S. He, L.M. Gerhardt, T.A. Holderried, M. Seifert, et al. 2016. On-demand erythrocyte disposal and iron recycling requires transient macrophages in the liver. *Nat. Med.* 22:945–951. https://doi.org/10.1038/nm.4146

Tsujioka, H., T. Imanishi, H. Ikejima, A. Kuroi, S. Takarada, T. Tanimoto, H. Kitabata, K. Okochi, Y. Arita, K. Ishibashi, et al. 2009. Impact of heterogeneity of human peripheral blood monocyte subsets on myocardial salvage in patients with primary acute myocardial infarction. *J. Am. Coll. Cardiol.* 54:130–138. https://doi.org/10.1016/j.jacc.2009.04.021

Weber, G.F., B.G. Chousterman, I. Hilgendorf, C.S. Robbins, I. Theurl, L.M. Gerhardt, Y. Iwamoto, T.D. Quach, M. Ali, J.W. Chen, et al. 2014. Pleural innate response activator B cells protect against pneumonia via a GM-CSF-IgM axis. *J. Exp. Med.* 211:1243–1256. https://doi.org/10.1084/jem.20131471

Wicks, I.P., and A.W. Roberts. 2016. Targeting GM-CSF in inflammatory diseases. *Nat. Rev. Rheumatol.* 12:37–48. https://doi.org/10.1038/nrrheum.2015.161

Wu, L., S. Ong, M.V. Talor, J.G. Barin, G.C. Baldeviano, D.A. Kass, D. Bedja, H. Zhang, A. Sheikh, J.B. Margolick, et al. 2014. Cardiac fibroblasts mediate IL-17A-driven inflammatory dilated cardiomyopathy. *J. Exp. Med.* 211:1449–1464. https://doi.org/10.1084/jem.20132126